2020-01-01

Supra-Salt Syndepositional Folding Within The Jurassic Morrison Formation, Big Gypsum Valley, Colorado

Alondra Soltero
University of Texas at El Paso

SUPRA-SALT SYNDEPOSITIONAL FOLDING WITHIN THE JURASSIC MORRISON FORMATION, BIG GYPSUM VALLEY, COLORADO

ALONDRA SOLTERO

Master's Program in Geology

APPROVED:

Richard Langford, Ph.D., Chair

Katherine A. Giles, Ph.D.

Terry Pavlis, Ph.D.

Geoffrey B. Saupe, Ph.D.

Stephen L. Crites, Jr., Ph.D.
Dean of the Graduate School

Dedication

To my family, who has supported my pursue for a higher level of education and my passion of science.

SUPRA-SALT SYNDEPOSITIONAL FOLDING WITHIN THE JURASSIC MORRISON FORMATION, BIG GYPSUM VALLEY, COLORADO

by

ALONDRA SOLTERO, B.S.

THESIS

Presented to the Faculty of the Graduate School of

The University of Texas at El Paso

in Partial Fulfillment

of the Requirements

for the Degree of

MASTER OF SCIENCE

Department of Geological Sciences

THE UNIVERSITY OF TEXAS AT EL PASO

May 2020

Acknowledgements

This thesis would not have been completed without the constant support and faith of my parents, Alejandro and Silvia Soltero. From a young age, they taught me to strive for perfection in everything I do and encouraged me whenever I felt overwhelmed or lost. Secondly, the support from my siblings, Alejandra and Gael. They remind me to have fun with my work and enjoy listening to my geologic knowledge even when they do not fully understand it. My inspiration to become a geologist came from my aunts, Daniela and Adriana, who worked alongside geologists in the petroleum industry as mechanical engineers. They opened my mind to the possibility of a career that involved my passion for the outdoors and science.

The creation of this thesis and underlying work would not have been possible without the guidance from my advisor and committee member, Richard Langford and Katherine Giles. Richard Langford, who challenged me every step of the way to think outside the box and see the bigger picture. His incredible knowledge and positive attitude are an inspiration to me as a future geologist. Katherine Giles, who taught me the value of learning and striving for perfection in everything I set out to accomplish.

Field assistance from fellow UTEP colleagues, Ezequiel Moreno, Eddie Zuniga, and Julia Astromovich. They contributed towards the collection of the data that was used within this thesis and helped me remain safe while hiking in Gypsum Valley, Colorado.

The financial support from the sponsors of the Institute of Tectonic Studies Salt-Sediment Research Consortium at The University of Texas at El Paso, and the donors for the research grants given by the West Texas Geological Society, Geological Society of America (GSA) and American Association of Petroleum Geologists (AAPG). Their support helped me complete my field work and utilize at the software I needed to complete my research.

I want to thank Nila Matsler, who's organizational assistantship and vigor pushed me to complete my work and remain on task as important deadlines approached. Her friendship, fun personality, encouragement, and constant support helped me get to where I am today.

Abstract

The Paradox Basin, along the Utah and Colorado border, exposes salt diapirs that form elongate "salt walls". Most exposures of sediments that were deposited during salt movement are hundreds of meters from the contacts. However, in the southeastern part of the Gypsum Valley diapir, a set of tight folds within the Jurassic Morrison Formation are preserved along the diapir margins where they overlie salt. These are best exposed at the southeastern end of Big Gypsum Valley. Previous interpretations suggested that the Morrison Formation folding and faulting occurred during dissolution of the diapir. However, field mapping reported here reveals that the Morrison Formation was deposited on the salt and the beds folded during deposition due to the movement of the underlying salt.

Detailed maps and 3D outcrop models of one presumed paleo-canyon, and four areas where folds are well exposed, show anticline-syncline couples and sub-horizontal Morrison beds in contact with the salt. The lower unit of the Morrison onlap the tilted strata flanking the diapir and the folded strata are found in the third stratigraphic unit. The onlap indicates continued subsidence of the flanking minibasins that exceeded the rate of deposition. Correlated stratigraphic sections across the folds show that Morrison strata thin and onlap the flanks of synclines. Indicating that thickening in synclines is a depositional phenomena rather than structural thickening through deformation after deposition. Basal Morrison strata in direct contact with Paradox gypsic caprock contain diapir-derived clasts, reflecting erosion of the diapir margin by the first channels that flowed there. On the southeastern section of the study area, the Morrison Formation incises at least 4 m into the underlying strata and is inferred to be the eroded remnant of a paleo canyon. The canyon is incised into upturned Pennsylvanian rocks that form a "megaflap" that must have formed a topographic high during Morrison deposition. The megaflap underwent erosion during salt-tectonic uplift prior to Morrison deposition. The lack of faulting in some areas indicates that much of the Morrison is in place and has not been dropped into its present location through diapir dissolution collapse as has been previously believed.

The findings contribute to creating models that try to define the resulting stratigraphy when salt is the main driver of sedimentation patterns. Potential reservoirs can be delineated on both sides of the diapir margin within the folded strata. Attaining a better understanding of the observed geometries will also serve as a basis for offshore exploration, where seismic imaging of salt diapirs is poor, making drilling hazardous for the equipment and employees involved.

Table of Contents

Acknowledgements v

Abstract vi

Table of Contents vi

List of Tables iix

List of Figures x

Introduction 1

Purpose 1

Background 1

Hypothesis 3

Study Area 4

Regional Setting: Geology and Tectonics of the Paradox Basin 9

Gypsum Valley 10

Salt Tectonism 13

Morrison Formation 16

Methods 19

Results 22

Area A 22

Area B 29

Area C 37

Area D 39

Area D 43

Petrographic Analysis 44

Sample MSw-A 45

Grains 45

Cement 47

Porosity 49
Samples MSw-B1 and MSw-B2 49
MSw-B1: Grains 50
MSw-B1: Cement 50
MSw-B1: Porosity 51
MSw-B2: Grains 52
MSw-B2: Cement 52
MSw-B2: Porosity 53
Comparison with Previous Studies 54
Discussion 57
Area A: Paleo-canyon 57
Salt Margin Folds 58
Area D: Folds in the Brushy Basin 60
Paleocurrent Measurements 61
Thin Sections 62
Conclusions 64
References 66
Vita 72

List of Tables

Table 1: Sample MSw-A 49

Table 2: Sample MSw-B1 53

Table 3: Sample MSw-B2 55

List of Figures

Figure 1: Termination of Passive Diapir Rise Model 3
Figure 2: Crestal Collapse Diapir Model 3
Figure 3: Location map of the Paradox Basin 5
Figure 4: Geologic Map of study area, Southeastern Gypsum Valley 7
Figure 5: Stratigraphy of Gypsum Valley 8
Figure 6: Salt Shoulder Schematic 15
Figure 7: Regional Depth-Converted Seismic Profile 20
Figure 8: Big Gypsum Valley - Study Areas 21
Figure 9: Area A – Geologic Map 23
Figure 10: Area A – 3-D Model 24
Figure 11: Area A – 3-D Model Paleocanyon Incision 24
Figure 12: Area A – Stratigraphic Correlation 27
Figure 13: Area A – Diapir-derived Clasts 27
Figure 14: Geologic Map – Paleocurrent Data 28
Figure 15: Area B – 3-D Model 29
Figure 16: Site B.1 – 3-D Model 30
Figure 17: Area B – Geologic Map 30
Figure 18: Site B.1 – Stratigraphic Correlation 31
Figure 19: Site B.2 – Stratigraphic Correlation 35
Figure 20: Area B – Diapir-derived Clasts 35
Figure 21: Area B – Cross-section Profile 36
Figure 22: Area C – Geologic Map 37
Figure 23: Area C – 3-D Model 38
Figure 24: Area D – Geologic Map 40
Figure 25: Area D – 3-D Model 41
Figure 26: Area D – Brushy Basin Pebbly Conglomerate 42
Figure 27: Area D – Brushy Basin Cross beds 42
Figure 28: Area D – Brushy Basin Cross beds Continue 42
Figure 29: Area E – Geologic Map 43
Figure 30: Sample MSw-A: Mud and Silt Grains 45
Figure 31: Sample MSw-A: Gypsum Grain 45
Figure 32: Sample MSw-A: Quartz and Chalcedony Grains 46
Figure 33: Sample MSw-A: Calcite and Microcline Grains 46
Figure 34: Sample MSw-A: Cements 47
Figure 35: Sample MSw-A: Porosity 49
Figure 36: Sample MSw-B1: Calcite and Quartz Grains 50
Figure 37: Sample MSw-B1: Calcite Cement 51
Figure 38: Sample MSw-B1: Dolomite Cement 51
Figure 39: Sample MSw-B1: Porosity 51
Figure 40: Sample MSw-B2: Dolomite Cement 53
Figure 41: Sample MSw-B2: Cements 53
Figure 42: Sample MSw-B2: Clay Cement 53
Figure 43: Paleocurrent Data Map by Claire Bailey 53
Figure 44: Possible Reservoir and Trap Locations Schematic 60

Introduction

Purpose

This study analyses the sedimentology, stratigraphy and deformational history of folded Morrison Formation exposed at the southern end of the Gypsum Valley salt wall in order to constrain the style and timing of deformation at the end of passive diapirism. Most previous studies of the interactions of salt and sediment have relied on outcrops at least a kilometer from the diapir margin (Hazel, 1994; Banham and Mountney, 2013; Venus et al., 2015). However, in Gypsum Valley, exposures document deposition adjacent to and on top of the diapiric salt. Sediment deposited on top of the salt on the diapir has been folded (Heness, 2016; McFarland, 2016; Ronson, 2018). The dynamics that shape these folds are uncertain, but growth strata within the synclines demonstrate that they formed syndepositionally (Heness, 2016; McFarland, 2016; Ronson, 2018). Furthermore, the currently accepted models for the Paradox Basin diapirs seem to be incompatible with the observed syncline.

Background

Beginning in 2014, the Institute for Tectonic Studies at the University of Texas at El Paso (UTEP) has conducted studies within the Paradox Basin, with Gypsum Valley, Colorado, as a primary focus. Early studies of this region indicated that salt could be observed in contact with overlying sediment (Stokes and Phoenix, 1948; Elston et al., 1962; Cater and Craig, 1970; Ge et al., 1996). More recent studies conducted by UTEP graduate students have also documented syndepositional halokinetic deformation of sediment in contact with the caprock of the Gypsum Valley diapir (Heness, 2016; Mast, 2016; McFarland, 2016; Ronson, 2018). Deformed strata range in age from Late Triassic to Late Jurassic.

The first detailed geologic maps of the Gypsum Valley salt diapir **(Fig. 3, 4)** noted a set of tight folds within the Late Jurassic Morrison Formation that are preserved along the margins of Big Gypsum Valley in the southeastern end of the diapir **(Fig. 3, 4)** (Stokes and Phoenix, 1948; Shawe, 1970). These are most evident at the southeastern end and get progressively more open to the northwest **(Fig. 4)**. Because the Morrison Formation has been assumed to be the first strata to cover the diapir after the cessation of diapirism, most workers have assumed that similar features in other diapirs are related to late stage salt dissolution in the Neogene (Gutiérrez, 2004; Guerrero et al., 2015). Other authors have ascribed similar folding in other diapirs as related to regional tectonic compression during the Laramide Orogeny (Baars and Stevenson, 1981; Trudgill, 2011; Rasmussen and Rasmussen, 2016; Grisi, 2018). However, the synclines are oriented parallel to the diapir margin and follow the curve of the southeast termination, suggesting that they might be related to salt-related deformation rather than regional tectonism.

An understanding of the stresses that existed during folding may allow a determination as to whether regional tectonism, sat-related tectonism, or dissolution was important. As exposure is good, the possible stresses that formed the folds can be constrained.

The accepted models for the Paradox Basin diapirs interpret the caprock of the salt diapir as a rigid plug (Ge et al., 1996; Ge and Jackson, 1998; Gutiérrez, 2004; Trudgill, 2011; Guerrero et al., 2015) **(Fig. 1)**. After the cessation of diapirism, the new sediment is deposited as horizontal beds above it, possibly onlapping irregularities, but with otherwise uniform thickness. This model does not fit field observations because the Morrison Formation in direct contact with the top of the salt diapir is folded. The second event in this model shows a buried salt diapir that undergoes dissolution of the underlying salt, which causes a collapse of the overlying layers into the diapir through a series of fault forming grabens or half grabens (Ge et al., 1996; Ge and Jackson, 1998;

Gutiérrez, 2004; Trudgill, 2011; Guerrero et al., 2015) **(Fig. 2)**. Paradox Basin folds have been described in the sediments resting on diapir caprock, but have been interpreted as Eocene features related to the Laramide Orogeny (Ge, 1996) or Neogene folds related to the dissolution of diapirs (Gutiérrez, 2004; Guerrero et al., 2015). It has only been recently that these folds have been recognized as syndepositional.

Hypothesis

This thesis addresses the study of the folds in the Morrison Formation along the margins of Gypsum Valley by addressing the following hypotheses.

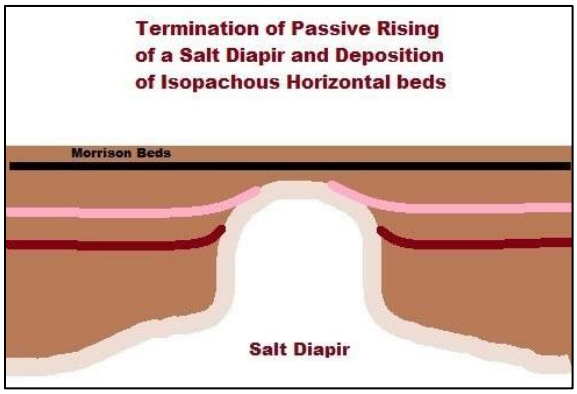

Figure 1: The currently accepted model showing the termination of passive rising of a salt diapir and the deposition of isopachous horizontal beds above it.

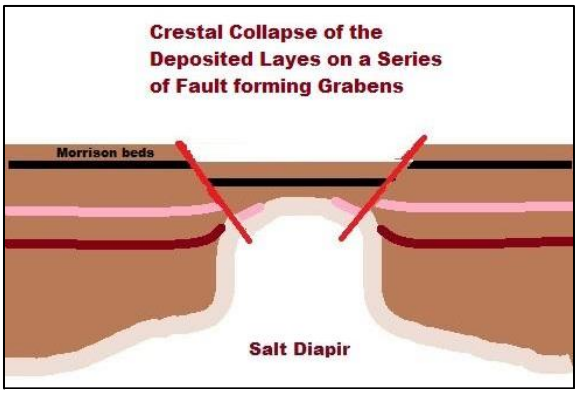

Figure 2: Continuation of the first model (Fig. 1), showing the crestal collapse of deposited layers on a series of fault forming grabens due to the dissolution and subsidence of the diapir.

Question 1: What is the relationship between the Morrison Formation and the salt diapir?

1. Hypothesis – The Morrison Formation was deposited on the salt, eroding the surface of the exposed diapir.

    1. Test 1 – Diapir derived clasts should be found within the Morrison beds in contact with the salt diapir.

    2. Test 2 – Detailed mapping along the diapir margin and synclines should show patches of the Morrison Formation in direct contact with the salt. Stratigraphy

should be correlatable to the Morrison strata on the margin of the adjacent areas flanking the diapir.

Question 2: When and how did the folds along the diapir margin form?

2. Hypothesis – The Morrison Formation above the salt folded during deposition due to the movement of the underlying salt.

    1. Test 1 – Morrison beds should show a lateral change in thickness, thickening into the axes of synclines and thinning on anticlines. Beds may onlap on salt or underlying strata on the flanks of synclines.

    2. Test 2 – Beds may have different and local facies within synclines.

Study Area

The study area is in Big Gypsum Valley, the southeastern end of Gypsum Valley, covering approximately 64 km^2 (**Fig. 3, 4**). The area exposes the contact between the diapiric Paradox Formation and the Morrison Formation, where a set of tight folds within the Morrison Formation are preserved along the diapirs' margins. **Figure 4** outlines the five key sites of exploration for this study, labeled A through E, where field observations, 3D models, stratigraphic correlations and/or rock sampling were made, and the location of the SW-NE seismic profile line published by Rowan et al. (2016).

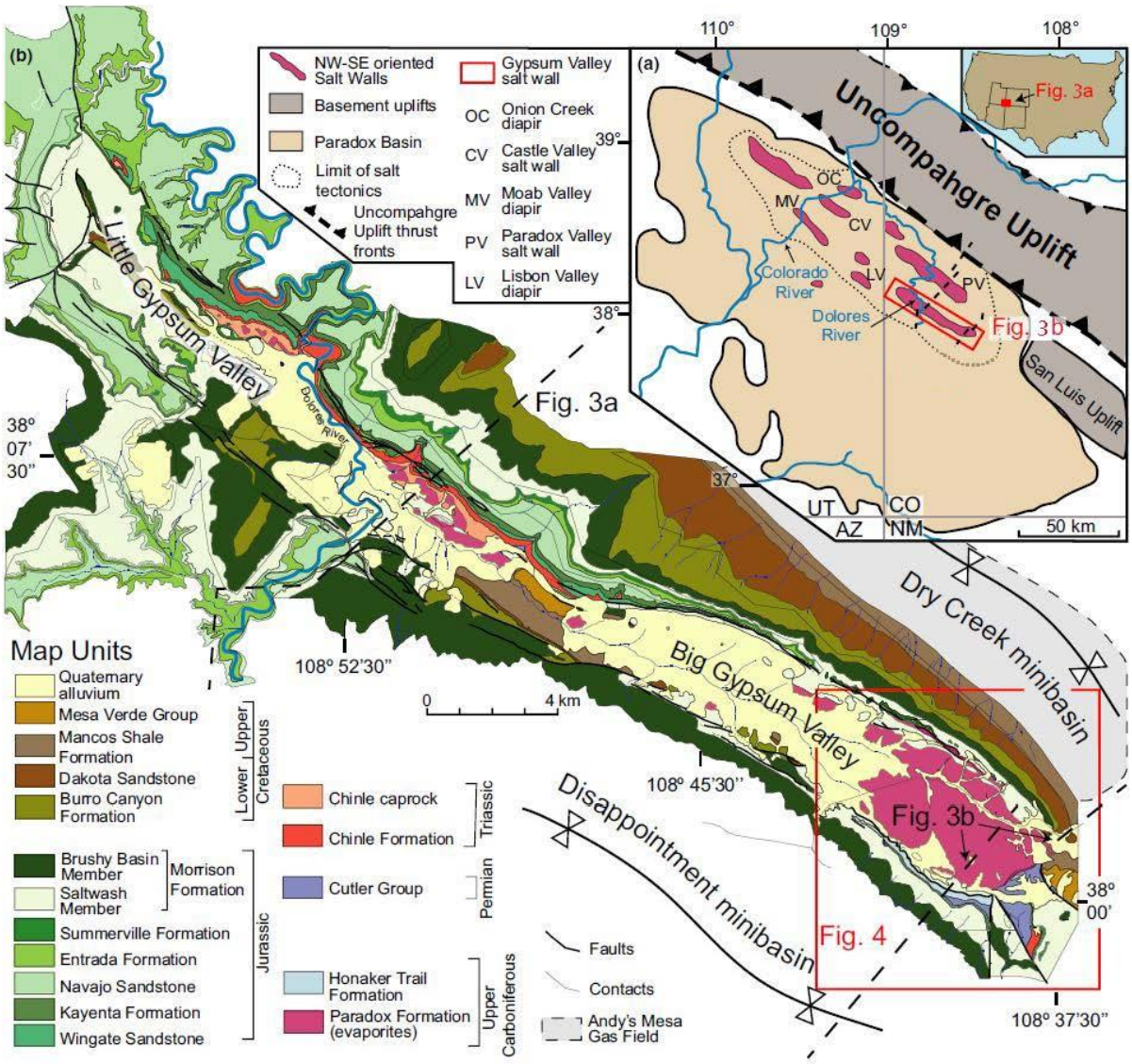

Figure 3: Location map: (a) Paradox Basin and its major salt walls (after Shoemaker, Case, and Elston, 1958); (b) geologic map of Gypsum Valley salt wall. The red outlines indicate in (a), the location of Fig. 3b and (b), the study area shown in Fig 4. Edited from Escosa et al. 2019.

In Big Gypsum Valley, the salt diapir is exposed in the center of the valley as a series of ashy-gray rounded hills. These consist primarily of gypsum and mixed outcrops of carbonates and black shales from the Pennsylvanian Paradox Formation (Stokes and Phoenix, 1948; Cater, 1955a). Big Gypsum Valley can be subdivided into five structural domains based on the presence of four different faults in the area (**Fig. 4**) (Escosa et al., 2019). The first fault, located on the southwestern margin of the salt wall, is a WNW-ESW trending minor fault (Escosa et al., 2019). The fault

produces a ca. 80 m offset of the Paradox-Cutler contact, terminating at the base-Entrada unconformity (Escosa et al., 2019). This minor fault divides domain one into two subdomains, I' and I" (**Fig. 4**). Area D is found within the Escosa et al. (2019) zone I', where the upper member of the Morrison Formation, the Brushy Basin, is exposed and folded into an anticline-syncline couple. Unlike other areas along the rim of the salt wall, the Paradox Formation in area D is covered by Quaternary alluvium adjacent to the outcrops. However, tight folding and growth strata within the syncline are still evident. In zone I", the Salt Wash Member of the Jurassic Morrison Formation onlaps vertically dipping black shales of the Paradox Formation, incising at least 4 meters into the underlying megaflap at area A (**Fig. 4**). North of the megaflap, at area E, the Salt Wash Member tightly folds into a syncline and onlaps the salt diapir (**Fig. 4**).

The next set of faults, the western and eastern radial faults, cut the strata flanking the diapir at the southern corner, dividing zones I", II, and III (**Fig. 4**). These faults trend perpendicular to the diapir margin and decrease in offset southward away from the diapir. They terminate within the Mancos Shale and are 2.9 and 3.5 km long respectively (Escosa et al., 2019). In zone II, Jurassic strata in the northern part of the graben are folded into an anticline-syncline pair with sub-horizontal fold axes that trend parallel to the eastern bounding fault (Escosa et al., 2019). Unlike other folds found along the salt wall margin in Big Gypsum Valley, the folds in zone II are outside of the diapir and strike perpendicular to the margin. They were likely displaced by the western and eastern radial faults.

Further east of the radial faults, an inferred counterregional fault accommodates more than 1.5 km of throw close to the salt diapir, with the Honaker Trail Formation in the footwall and a thickened Upper Pennsylvanian-Cretaceous sequence in its hanging wall (**Fig. 4**) (Escosa et al., 2019). West of the counterregional fault, strata within zone III forms a moderately to gently

dipping panel over the plunging nose of the diapir with maximum dips of 45° close to the diapir (**Fig. 4**) (Escosa et al., 2019). To the east, zone IV forms the downthrown hanging wall of the counterregional fault (**Fig. 4**) (Escosa et al., 2019). Here, strata are generally sub-horizontal but with a broad, gentle syncline crossing the counterregional fault near its termination against the diapir (Escosa et al., 2019).

Lastly, on the northeastern flank of the diapir, a northeast-southwest striking lateral normal fault within the Dakota Sandstone divides zones IV and V. In zone V, the Salt Wash Member folds into an anticline-syncline pair onlapping the salt diapir and vertically dipping Chinle Formation beds as part of areas B and C, forming a Morrison shoulder (**Fig. 4**).

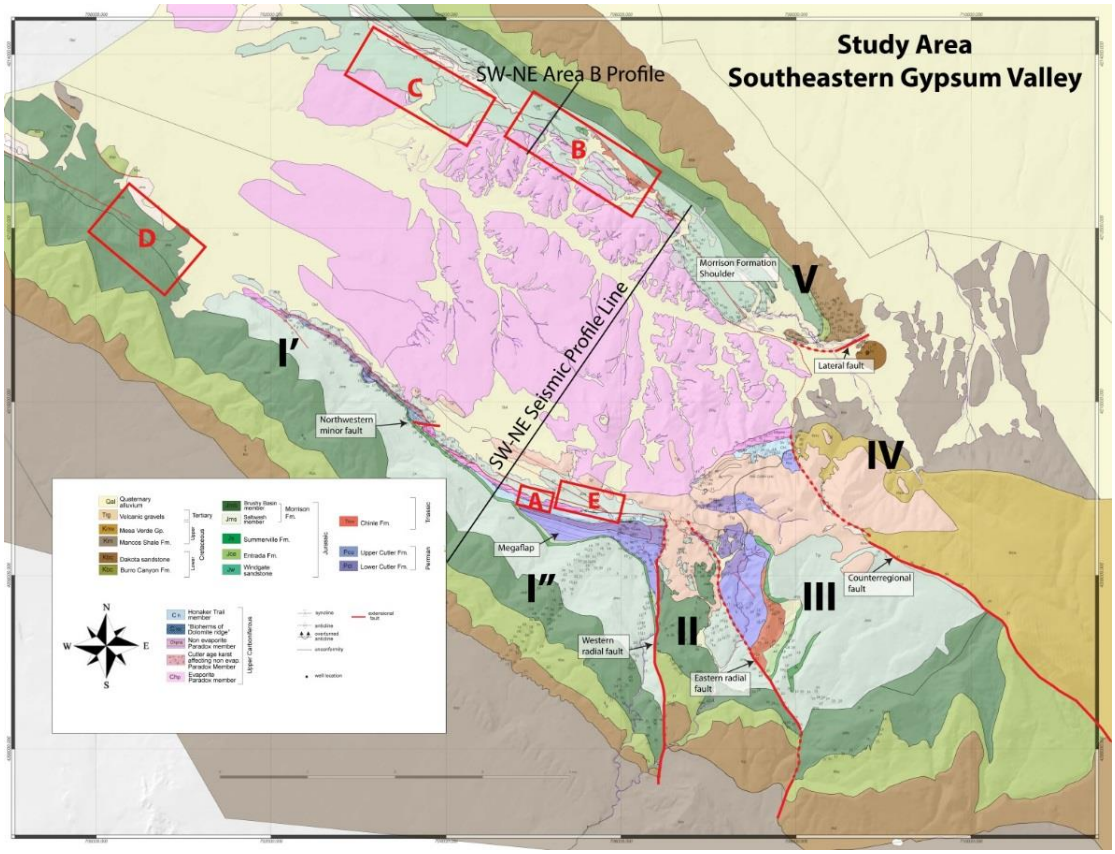

Figure 4: Geologic map of the study area, located at the SE end of the Gypsum Valley salt wall. The red squares, labeled A- E, outline the areas of interest where stratigraphic correlations, field observations, and/or rock sampling were made. The black line represents the SW-NE Seismic Profile Line made by Rowan et al. (2016) (Fig. 7).

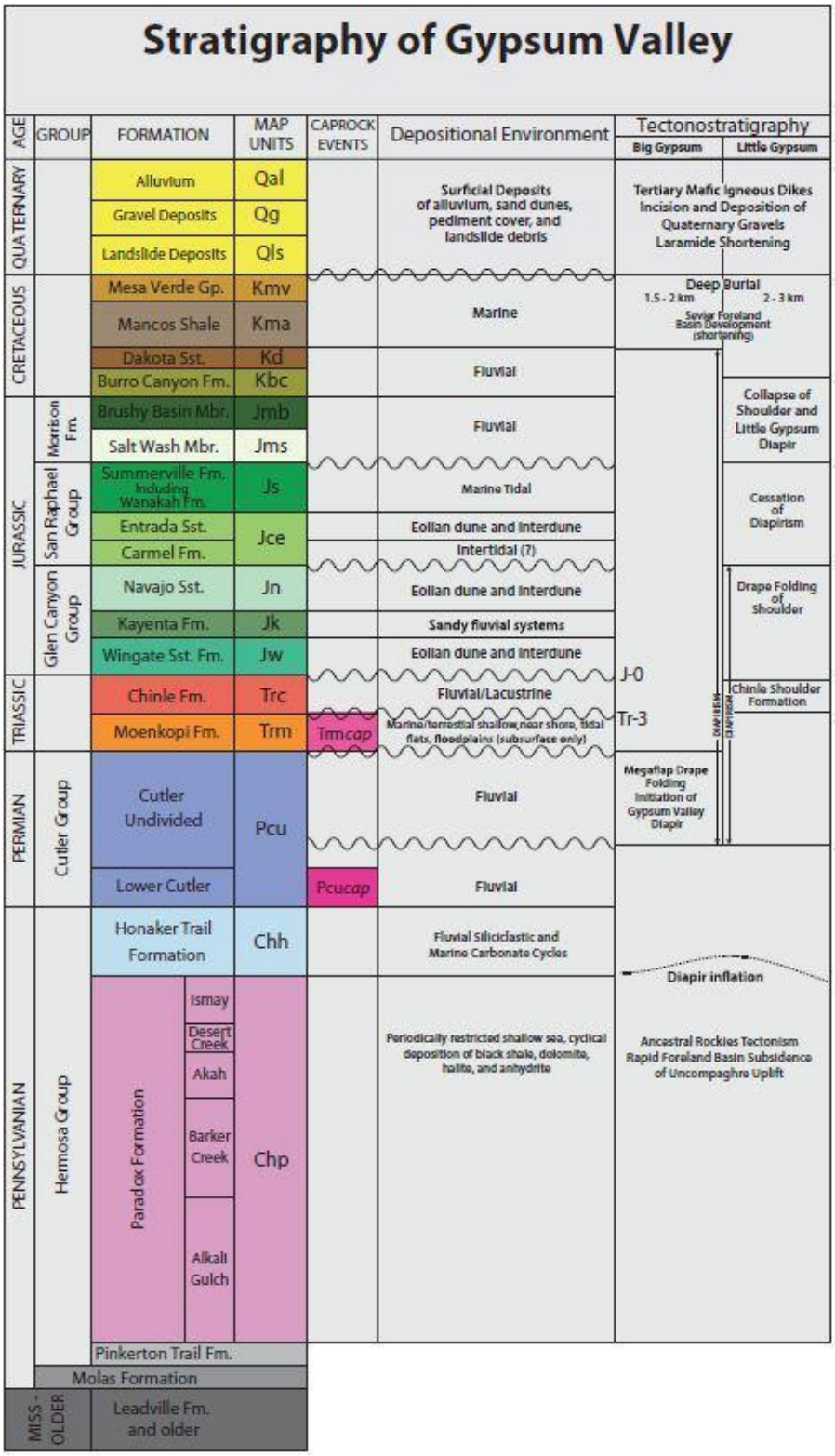

Figure 5: Strat units in the Paradox Basin at the Gypsum Valley area. The depositional environment, depositional events, and controls are after Stokes and Pheonix (1948), Doelling and Ross (1998), and Trudgill (2011). Key unconformities are also annotated (Shawe, 1970). Unit colors and abbreviations are kept for Fig. 9, 10, 17.

Regional Setting: Geology and Tectonics of the Paradox Basin

The Paradox Basin, located in southeast Utah and southwestern Colorado **(Fig. 3a)**, formed as a foreland basin southwest of the rising Uncompahgre Uplift and north of the Four Corners platform as a result of the Pennsylvanian-Permian Ancestral Rocky Mountain orogeny (Hanshaw and Hill, 1969; Baars and Stevenson, 1981; Kluth, 1986; Barbeau, 2003; Matthews et al., 2007; McFarland, 2016). The Ancestral Rocky Mountains are intracratonic block uplifts that formed in the southwest United States during Pennsylvanian time as a result of the collision between Laurasia and Gondwana during the assembly of Pangea (Kluth and Coney, 1981; White and Jacobson, 1983; Huntoon et al., 2002; Barbeau, 2003). The Paradox Basin is defined by the depositional extent of the layered evaporites of the Pennsylvanian Paradox Formation and measures ca. 300 km in length (northwest to southeast) and ca. 150 km in width (Condon, 2000; Trudgill, 2011; Whidden et al., 2014; Escosa et al., 2019).

The Paradox Basin is an asymmetric depression that accumulated thick deposits of halite, carbonates and organic-rich mudstone as a result of tectonic downwarping and simultaneous uplift along its northeastern border (Nuccio and Condon, 1996; Barbeau, 2003; Trudgill, 2011). Salt mobilization and diapiric rise began due to differential loading by the Pennsylvanian Cutler Formation derived from the Uncompahgre Uplift, the main proximal sediment source for the Pennsylvanian-Triassic sediments found within the northeastern part of the basin (Baars and Stevenson, 1981; Mack and Rasmussen, 1984). The northern part of the Paradox Basin is referred to as the Paradox fold and fault belt due to the series of roughly parallel, northwest-trending faults and salt-cored anticlines (Kelley, 1958; Nuccio and Condon, 1996).

Salt movement began at the end of the Pennsylvanian and passive diapirism started by early Permian time and continued as the Cutler, Glen Canyon, and San Raphael Groups were deposited

(Stokes and Phoenix, 1948; Doelling and Ross, 1998; Trudgill, 2011) **(Fig. 5)**. It was during the mid-Jurassic that cessation of diapirism is thought to have occurred and the Morrison Formation was deposited (Stokes and Phoenix, 1948; Shawe, 1970; Doelling and Ross, 1998; Trudgill, 2011) **(Fig. 5)**.

After the end of the Ancient Rocky Mountain tectonics and the Permian peak of salt tectonics, relatively minor shortening is believed to have occurred during the Sevier and Laramide orogenies, which was mostly in the form of reactivations and overprinting of structures including the salt walls (Baars and Stevenson, 1981; Trudgill et al., 2004). During the Laramide Orogeny, regional west-east shortening may have folded all of the diapirs and anticlines (Rasmussen and Rasmussen, 2016). Normal faults that commonly strike parallel to the salt walls were thought to be associated with salt dissolution in the Neogene (Trudgill, 2011). Diapir evaporites were exhumed during the Neogene due to the widespread incision seen in the Rocky Mountains and the Colorado Plateau (Rasmussen and Rasmussen, 2016). This, coupled with the relatively wetter climate of the Pleistocene, led to an increase in erosion, dissolution, and the subsequent collapse of the salt anticline roof strata, where an overburden of more than 3 km was eroded (Nuccio and Condon, 1996). The dissolution of salt along the crests of some anticlines in the Neogene has led to downfaulting and the development of grabens at the crests (Ge et al., 1996; Nuccio and Condon, 1996).

Gypsum Valley

The Gypsum Valley diapir, located in southwest Colorado, is the southernmost of the northwest-southeast trending salt structures found within the Paradox Basin (Cater and Craig, 1970). The salt wall is bounded on the northeastern side by the Dry Creek minibasin and on the southwestern side by the Disappointment minibasin, forming a breached anticline geometry that is almost 35 km long and from 2-3.5 km wide (Stokes and Phoenix, 1948; Cater, 1955b; Escosa et al., 2019) (**Fig. 3b**).

This anticline contains a large, northeast trending valley that has been thought to have attained its shape from the dissolution collapse of the top of the salt diapir (Stokes and Phoenix, 1948; Cater, 1955a; Cater and Craig, 1970; Trudgill et al., 2004). The strata dip away from the diapir and range from horizontal to vertical as a result of the rising salt and subsidence of the synclines flanking the diapir (Stokes and Phoenix, 1948; Shawe, 1968). Generally, older formations dip more steeply while the younger formations are successively deposited across the upturned and truncated edges of the older formations (Cater and Craig, 1970). The collapse of the axial part of the Gypsum Valley anticline is thought to have occurred in multiple stages, beginning with the down-faulting of the crests of the anticlines as grabens as a result of the Miocene uplift of the Colorado Plateau (Cater and Craig, 1970; Nuccio and Condon, 1996). It was this uplift that initiated the major stream incision and the associated breaching of salt cores (Cater and Craig, 1970; Nuccio and Condon, 1996).

The diapiric Paradox Formation makes up the core of Gypsum Valley salt wall and is flanked by Late Pennsylvanian through Lower Cretaceous strata (**Fig. 4**) (Stokes and Phoenix, 1948; Doelling and Ross, 1998; Trudgill et al., 2004). The gypsum, black shale, and dolomite of this formation crop out near the middle of the valley and along its margins as isolated low rounded hills (Cater and Craig, 1970).

Geographically, Gypsum Valley can be divided into two parts, marked by where the Dolores River cuts across the valley (Stokes and Phoenix, 1948). Little Gypsum Valley is located northwest of the Dolores River, and Big Gypsum Valley is to the southeast of the river (**Fig. 3b**). In Big Gypsum Valley, vertical to overturned strata as old as Pennsylvanian are exposed where erosion has penetrated the overlying Morrison Formation (Stokes and Phoenix, 1948). In Little Gypsum Valley, the Entrada, Summerville, and Morrison Formations outcrop along the valley

floor. Previous authors thought collapsed blocks of the Salt Wash Member of the Morrison Formation are in contact with the Paradox Formation (Cater and Craig, 1970). In contrast, McFarland (2015) and Heness et al. (2017) noted little faulting on the flanks of the diapir and inferred that Triassic Chinle strata were in depositional contact with the salt wall in Little Gypsum Valley.

The southeastern termination of the salt wall, at the southern end of Big Gypsum Valley, is the focus of this study. In this area, the two members of the Morrison Formation – the Brushy Basin and Salt Wash members – are well exposed at the surface. A combination of seismic reflection, well, and field data, depict an important asymmetry between the bounding minibasins of the study area (Amador et al., 2009; Rowan et al., 2016; Escosa et al., 2019). On the northeastern side, Upper Pennsylvanian to Permian strata are relatively thick and deeply buried, with a minor upturn near the diapir and a series of exposed folds along its margins (Escosa et al., 2019). The southwestern side is marked by Pennsylvanian strata that gradually thins and upturns to the near-vertical adjacent to the diapir to form a megaflap (Mast, 2016; Rowan et al., 2016; Deatrick, 2019; Escosa et al., 2019).

The diapir is believed to have first formed as a salt pillow (Escosa et al., 2019). Salt movement is thought to have begun with a breakout through the roof along its northeastern margin that allowed the diapir to rise and rotate the roof up to form a megaflap, that today is exposed along the southeast margin of the study area (**Fig. 4**) (Escosa et al., 2019). Subsidence along the breakout zone formed a counterregional fault that underlies the northeastern part of the study area, although this is not evident at the surface (**Fig. 4**). Salt breakthrough and the onset of passive diapirism is thought to have begun in the early Permian when erosion on the Mid-Cutler unconformity exposed the roof (Escosa et al., 2019). The evacuation of deep salt into the growing diapir produced diapir-

flaking depocenters, that today form the Disappointment and Dry Creek minibasins that flank the study area to the northwest and southeast respectively (**Fig. 4**) (Escosa et al., 2019). Doming of the diapir crest formed radial faults that segment the Morrison Formation and that were active until at least the Late Cretaceous (**Fig. 4**) (Escosa et al., 2019).

Salt Tectonism

Salt behaves in a ductile fashion when responding to regional tectonic stresses, differential loading, and a wide range of geologic conditions (Rowan and Vendeville, 2006; Hudec and Jackson, 2007). Therefore, regional tectonics play a large role in enhancing the movement and shape of salt diapirs (Hudec, 1995; Jackson et al., 1998; Trudgill, 2011).

The stratal geometries that flank passively rising salt walls typically range from halokinetic sequences to megaflaps, depending on the scale of near-diapir deformation. Halokinetic sequences are localized, unconformity-bound successions of growth strata that form as drape folds due to the interactions between the rate at which salt rises and the sediment-accumulation rate (Giles and Lawton, 2002; Rowan et al., 2003; Escosa et al., 2019). Megaflaps are sections of deep minibasin strata that gradually thin and upturn to near-vertical along the sides of diapirs (Giles and Rowan, 2012; Escosa et al., 2019).

Halokinetic sequences are ubiquitous in strata that are adjacent to passive salt diapirs and record the interaction of the rising salt and adjacent accumulating sediment (Giles and Lawton, 2002; Andrie et al., 2012). They are influenced by salt movement in or near the earth's surface and are bounded at the top and base by angular unconformities (Giles and Lawton, 2002). Halokinetic sequences form two structural and depositional end members; the hook and the wedge (Giles and Rowan, 2012). The hook is a narrow zone of deformation with an angular discordance greater than 70^{o}, mass wasting deposits, and abrupt facies changes (Giles and Rowan, 2012). On the other hand,

the wedge contains a broad zone of folding, low-angle truncation, and gradual facies changes (Giles and Rowan, 2012). Like parasequence sets, stacked composite halokinetic sequences (CHS) represent time scales equivalent to third order depositional cycles, where stacked hook halokinetic sequences from tabular CHS and wedge halokinetic sequences form tapered-CHS (Giles and Rowan, 2012).

Salt shoulders have been identified throughout Gypsum Valley but are most notable in Little Gypsum Valley (Heness, 2016; McFarland, 2016; Ronson, 2018). These are best defined as low angle segments of the salt-sediment interface where the margin of a passive diapir steps abruptly inboard (Heness, 2016; McFarland, 2016). A salt shoulder **(Fig. 6)** can be divided into inboard and outboard segments (Heness, 2016; McFarland, 2016). McFarland (2015) documented in the Triassic Chinle Formation three wedge halokinetic sequences (WHS-1, WHS-2, WHS-3) that onlap one salt shoulder in Gypsum Valley, that were each locally bounded by angular unconformities less than 5° (McFarland, 2016). Each halokinetic sequence has ledge-forming channel-fill sandstones with local conglomerates forming at the base while wedges of slope-

forming, finer-grained silt-rich sandstones separate the channel sands and pinch out towards the diapir (Heness, 2016; McFarland, 2016).

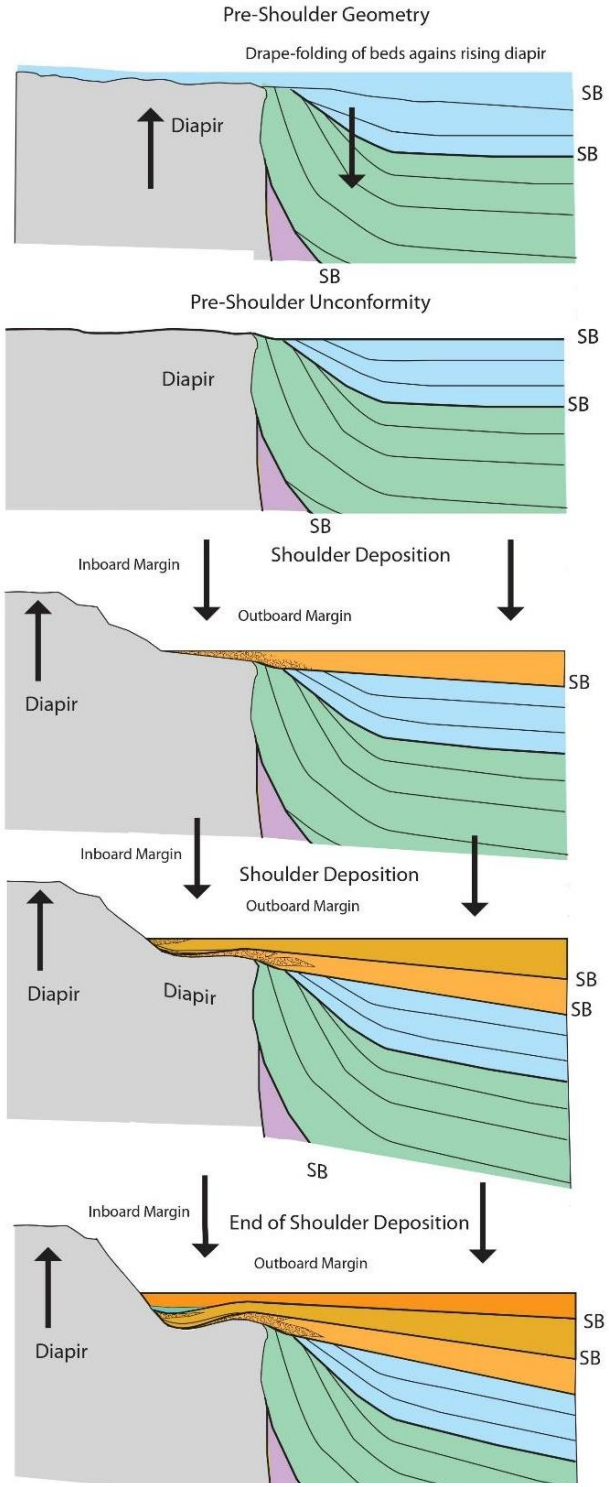

Figure 6: Schematic showing the formation of a salt shoulder and the resulting stratigraphic geometries.

Morrison Formation

The Jurassic Morrison Formation has long been famous for containing vertebrate fossils, most notably the large dinosaurs (Shawe, 1970). Its depositional environment ranges from eolian to fluvial and lacustrine (Nuccio and Condon, 1996). In the study area, the Morrison Formation consists of two members: the lower Salt Wash Member and the upper Brushy Basin Member (Cater and Craig, 1970; Tyler and Ethridge, 1983; Condon, 1992; Nuccio and Condon, 1996).

The Salt Wash Member is composed of sediment deposited in stream channels, flood plains, and in shallow lakes and ponds (Shawe, 1970; Tyler and Ethridge, 1983; Owen et al., 2015; Hartley et al., 2015). Regionally, the salt wash is thought to form a large fluvial fan that prograded north and east from a point near the Northwestern corner of Arizona (DeCelles and Currie, 1996; Owen et al., 2015). The Salt Wash Member is best described as a series of light-buff to rusty-red lenticular fine-grained sandstone layers that show scour and fill features and cross-bedding that is typical of fluvial channel sediments, intercalated with tabular reddish-brown, green and gray mudstones with scattered thin limestone beds (Stokes, 1944; Cater and Craig, 1970; Shawe, 1970; Tyler and Ethridge, 1983). In Gypsum Valley, the Salt Wash Member can be divided into four separate units that can be correlated throughout the valley (Bailey, 2018). The oldest unit (1) can be best described as a series of reddish brown to greenish gray floodplain mudstones and siltstones interbedded with sandy crevasse splay deposits (Bailey, 2018). They include fine to medium grained sandstones that are horizontally bedded, trough cross-bedded with ripple cross-strata, undulatory bedding, and episodic bioturbation (Bailey, 2018). Unit 2 is a cliff and ledge forming unit that consists of amalgamated, fine grained braided channel sandstones that have an erosional base with rip-up clasts (Bailey, 2018). Sandstones are dominantly trough cross-bedded to laminated with bioturbation at the top of the bed. Unit 3 is a slope-forming unit that includes

isolated meandering channel deposits (Bailey, 2018). These lenticular fine-grained sandstones show subhorizontal bedding with lesser amounts of massive and convoluted bedding as lateral accretion sets (Bailey, 2018). Lastly, unit 4 is a cliff-forming sandstone composed of laterally stacked meandering channel fill deposits, including fine grained sandstones with pebble to gravel sized conglomerates at the base (Shawe et al., 1968) (Bailey, 2018). These beds are dominantly sub-horizontally bedded to massive with minor amounts of soft-sediment deformation and convoluted bedding (Bailey, 2018). Like unit 3, these channels form lateral accretion sets, marking them as meandering channels (Bailey, 2018). Shawe (1968) used the top of the cliff in unit 4 to mark the top of the Salt Wash Member. However, Bailey (2018) included approximately 30 m of overlying mudstones into unit 4 and marked the top of the Salt Wash at the first pebbly sandstone of the Brushy Basin Member.

The Brushy Basin Member consists of multi-colored bentonitic shale and horizontally bedded and thinly laminated mudstones, rusty-red and red sandstone and conglomerates, and thin lenticular limestone beds and nodules (Stokes, 1944; Cater and Craig, 1970; Shawe, 1970; Kowallis et al., 1991; Hasiotis, 2004). This is the most widespread member of the Morrison Formation and it is known to contain silicified plant debris, silicified wood fragments in horizons, and dinosaur bones (Stokes, 1944; Shawe, 1970). The Brushy Basin member consists largely of the products of volcanic activity – mainly altered ash or bentonite that was reworked and mixed with sand and silt in varying extents (Stokes, 1944). In Gypsum Valley, the Brushy Basin Member has also been subdivided into three parts, named conveniently on the basis of their dominant color – the lower brown unit, the middle greenish gray unit, and the upper brown unit (Shawe, 1970). The lower brown unit is a transitional sequence of structureless reddish brown mudstone, lenticular sandstone and light-greenish-gray conglomerate strata with chert nodules similar in color and

lithology to that of the Salt Wash Member (Shawe, 1970). The middle green unit is characterized by dominant greenish-gray colors of mudstone and fine grained to coarse grained sandstone layers, with the highest proportion of conglomeratic sandstone than the underlying and overlying beds (Shawe, 1970). Lastly, the upper brown unit of the Brushy Basin Member is principally mudstone with minor proportions of sandstone, conglomeratic sandstone and conglomerate in discontinuous lenses (Shawe, 1970). Unlike the lower brown unit, this one contains more bentonitic material (Shawe, 1970).

Methods

In order to achieve the goals outlined in this study, high definition aerial imagery obtained from Google Earth was merged with the use of PhotoShop and then imported onto QGIS. These images were then combined with topographic maps on a tablet computer to be used for field observations. Field work concentrated on five areas, which contained important features in the Morrison Formation (**Fig. 8**). A total of 6 and 12 stratigraphic sections were measured on areas A and B, respectively, where the Morrison Formation was found in direct contact with salt, using a Jacob's Staff for bed thickness and Brunton Compass for bed orientation (**Fig. 9, 16**). These were georeferenced using a handheld GPS. The measured sections were digitized using PowerPoint and then correlated in Illustrator for further interpretation. Beds were correlated using the imagery, stratigraphic sections and field map. Geologic maps showing the correlated beds and interpreted lithologies were created for each set of folds.

Paleocurrent data were also gathered in order to expand our knowledge on the flow direction for the southeastern end of Big Gypsum Valley, which could potentially have an impact in the observed geometries. This information is displayed in Rose Diagrams and tied to the regional work done by Claire H. Bailey.

3-D outcrop models for four of the study areas were also created using photogrammetry with imagery obtained with a drone camera with the help of graduate student David F. Lankford. Phone apps Drone Deploy and DJI GO 4 were used to map the flight paths for the drone and these flights were flown in automomous mode. For most of the models, we flew the drone at an elevation of 220 ft to obtain nominal pixel resolution of 0.8 in/px The models were georeferenced using GPS logs of the drone with no ground control Sandstone channels within the Salt Wash and Brushy Basin Members of the Morrison Formation were traced on these models using line tools in Agisoft

Metashape Professional in hopes of better displaying the lateral change in bed thickness, the correlation of channels across the valley, and the overall geometry and distribution of the folds in direct contact with the salt diapir.

Hand samples of the basal strata of the Morrison Formation and diapir caprock were gathered from areas A and B (**Fig. 8**) so diapir derived clasts could be point counted in thin section using carbonate and feldspar stains. Additionally, a blue dye was used to study the permeability of the gathered samples. The rocks were first cut using a rock saw on campus and then sent to Spectrum Petrographics Incorporation for thin section preparation.

A cross-section of area B was created using the qProf plug-in in QGIS to acquire a topographic profile along the anticline-syncline pair where the Morrison Formation onlaps the salt diapir and near-vertical Chinle Formation. The units were projected onto the profile and then annotated in Illustrator using the dips on the detailed map.

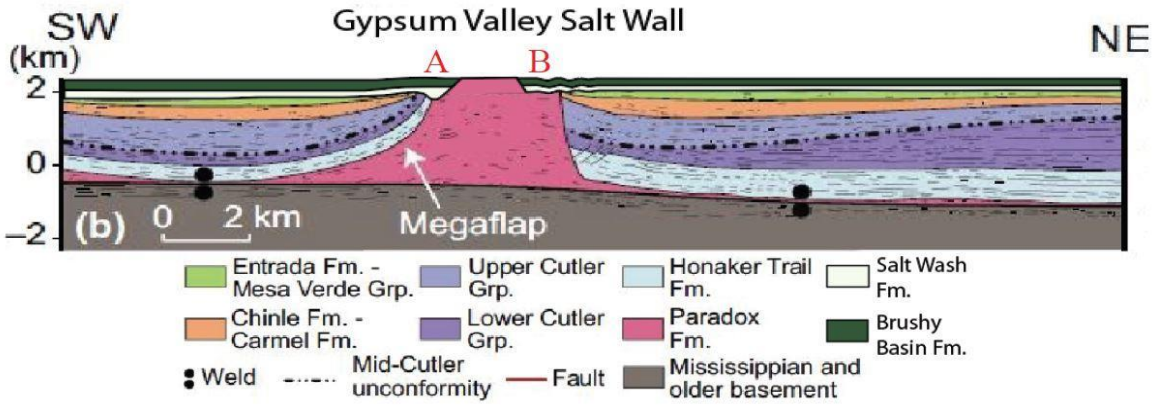

Figure 7: The regional depth-converted seismic profile in the SE Paradox Basin, as shown in the Study Area map (Fig. 4). Modified from Rowan et al. (2016) and Escosa et al. (2019), outlining the relationship between the Morrison Formation and the underlying units in areas A and B.

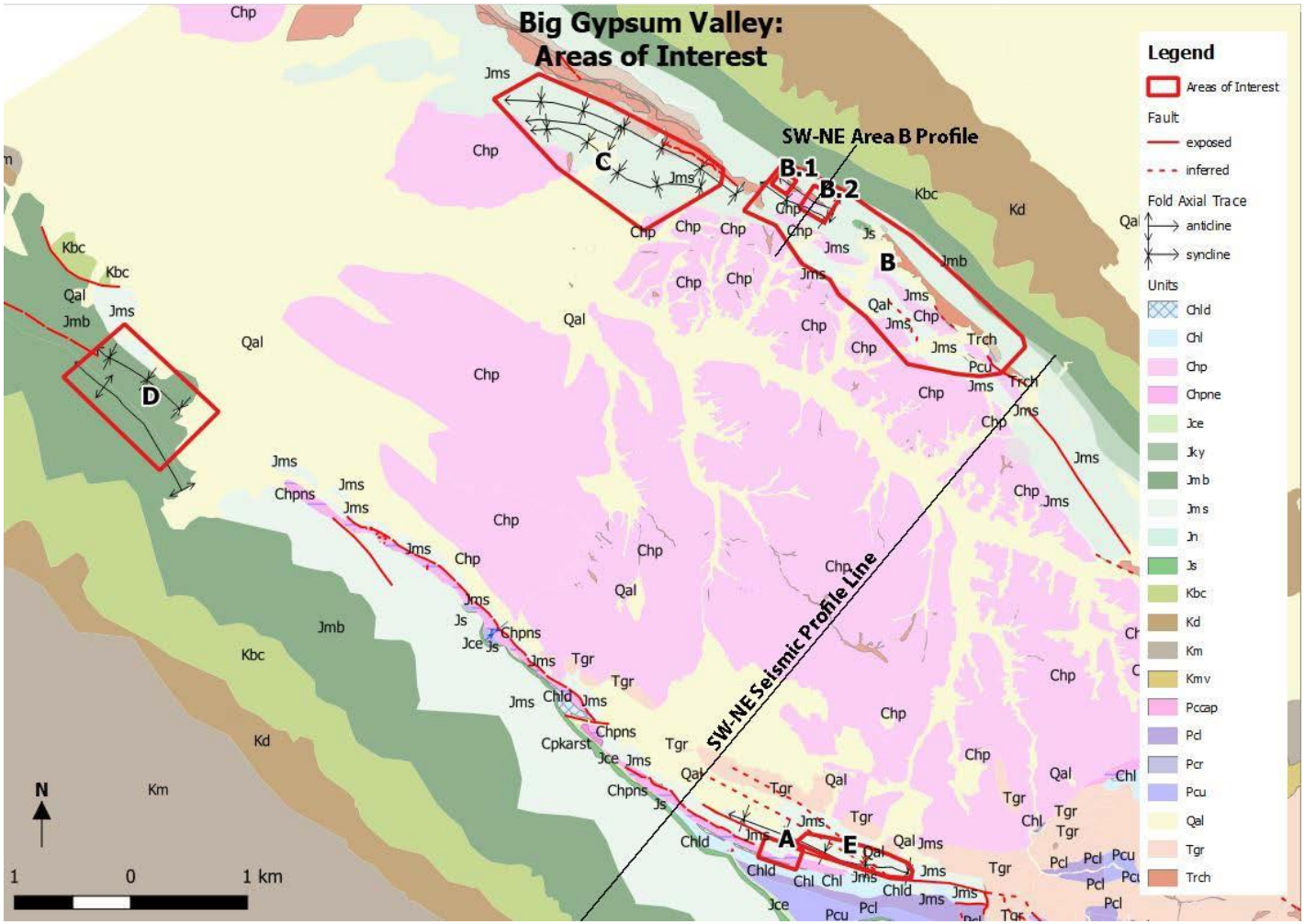

Figure 8: The locations and subdivisions of the five areas of interest within Big Gypsum Valley for this study, including areas A-E (where B is subdivided into B.1 and B.2). The seismic profile line by Rowan et al (2016) (Fig. 7) and Area B cross-section are also shown above. The map units are based on the stratigraphic column in Fig. 5.

Results

Five key sites were chosen for detailed study based on outcrop accessibility, quality, and importance for interpretation. Areas A-C and E showed good outcrop exposure where the Salt Wash Member of the Morrison Formation was folded and in direct contact with the salt diapir. Area D showed exposures of Brushy Basin folds where the Paradox Formation is covered by Quaternary alluvium.

Figure 7 shows the regional cross section developed from the depth-converted seismic profile in the southeastern Paradox Basin, which was modified from Rowan et al. (2016) and Escosa et al. (2019) to better display sites A and B of this study and the observed relationships between the Morrison Formation and the underlying salt. Geology in the figure was projected from detailed geologic mapping by several researchers and was presented in Escosa et al. (2019) (**Figs. 7, 8**). The line cuts across study areas A and B, located on the southwestern and northeastern diapir margins respectively (**Figs. 7, 8**). At area A, the Morrison Formation incises into the older units of the Megaflap and onlaps upturned beds of the Paradox Formation shales and dolomites. At area B, which can be divided further into sites B.1 and B.2 (**Fig. 8**), the Morrison Formation is found folded and in direct contact with the salt diapir. At area C, located on the northeastern flank of the salt wall, the Salt Wash Member of the Morrison Formation wraps around the exposed diapir, forming a tight syncline-anticline-syncline fold system parallel to the diapir's margins (**Fig. 8**). Area D contains Brushy Basin beds that fold into a syncline-anticline pair towards the cliff-side to the southwest of the diapir (**Fig. 8**). At area E, located north of area A, the Morrison Formation onlaps the salt and is tightly folded into a syncline (**Fig. 8**).

Area A

Six stratigraphic sections were measured in area A (**Fig. 9**). A 3-D model of the area was also created for this outcrop, which is located on the top of a ridge that exposes the megaflap along the southern tip of the salt wall (**Fig. 10, 11**). The site exposes a rocky hill of Morrison that dips

into the diapir at 43° to the North, striking 276°. The Morrison Formation rests on vertically dipping black shales. These have been interpreted as shales of the Paradox Formation that were originally interbedded with salt (Deatrick et al.; Mast, 2016). The black shales are also interpreted as having originally formed the roof of the diapir, which was then tilted to vertical as part of a megaflap that runs along the southwestern side of the southern end of the diapir (Mast, 2016; Escosa et al., 2019). The eastern and southern edges of the Morrison outcrop are an abrupt erosional cliff (**Fig. 10**). The western side shows onlap of Morrison strata against the black shales, and the Morrison strata are eroded into a slope (**Fig. 11**)**.** To the north, the Morrison dips steepen and merge into a larger Morrison outcrop that forms a dip slope along the northern side of the ridge. This same slope also forms the southern side of the syncline mapped in area E, although strata between the two areas are offset on a fault that displaces area E down into the diapir (**Fig. 8**).

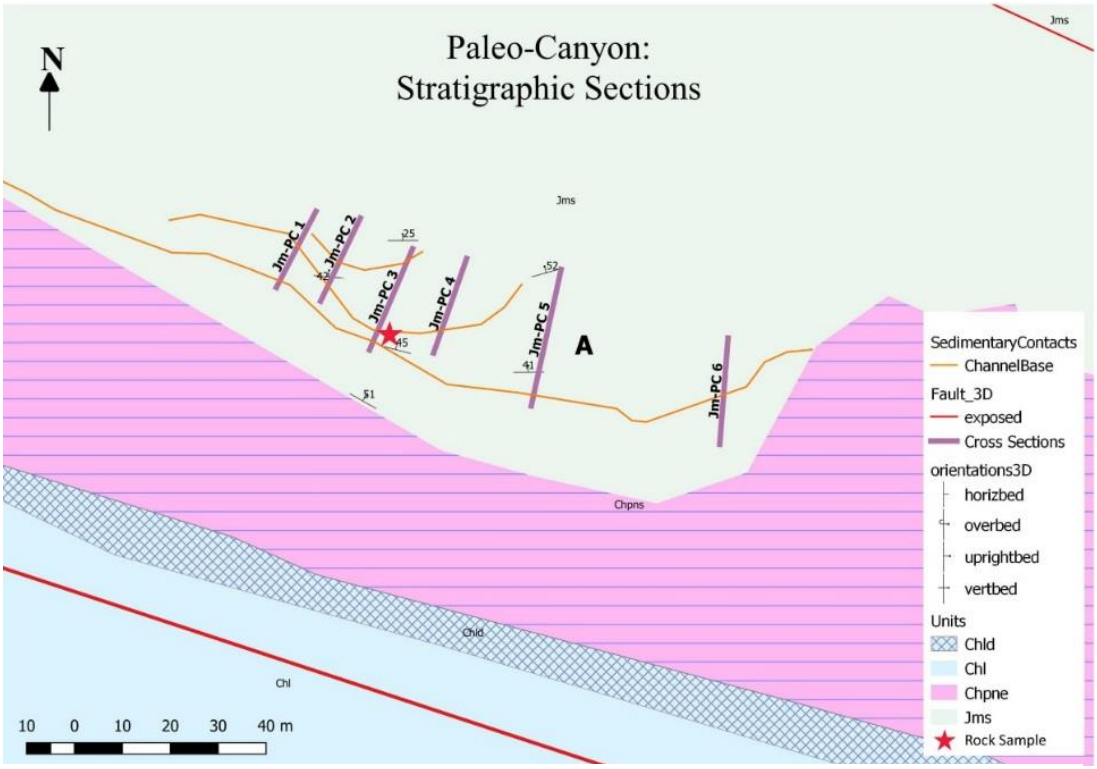

Figure 9: Southwestern margin of the study area showing the location of the strat sections measured in area A, the Paleo Canyon. The unit abbreviations and colors match those in Fig. 5. The star shows the location of rock sample MSw-A.

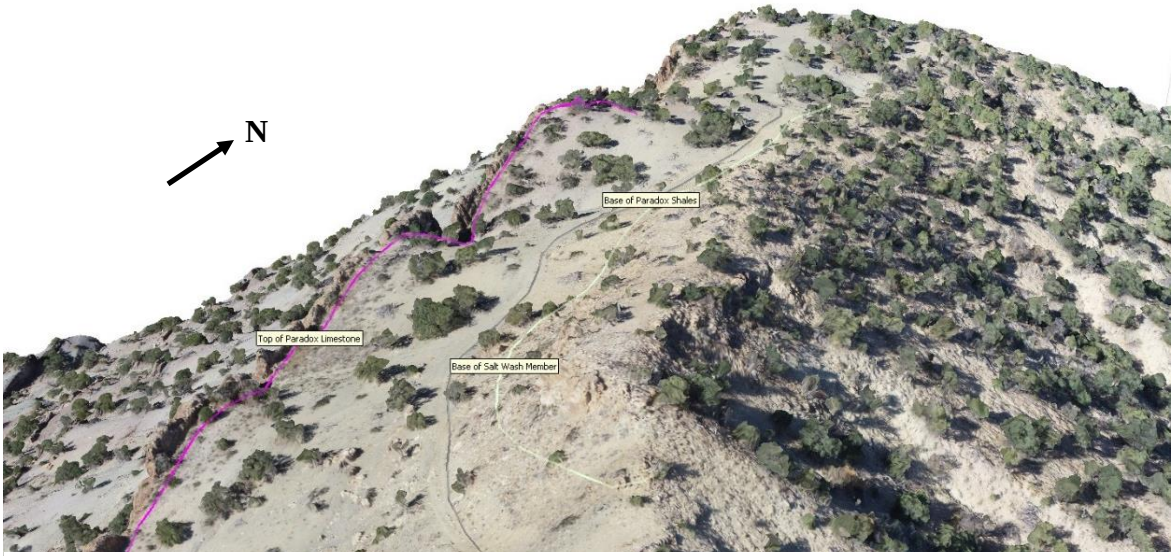

Figure 10: Perspective view of the 3D model of the Paleo Canyon in area A of this study looking NW, which has an erosional cliff-face to the east and south. The pink line shows where the vertical Paradox Limestone is exposed. The light green line marks the base of the Salt Wash Member of the Morrison Formation, which is incising into the vertical Paradox Shales (gray boundary).

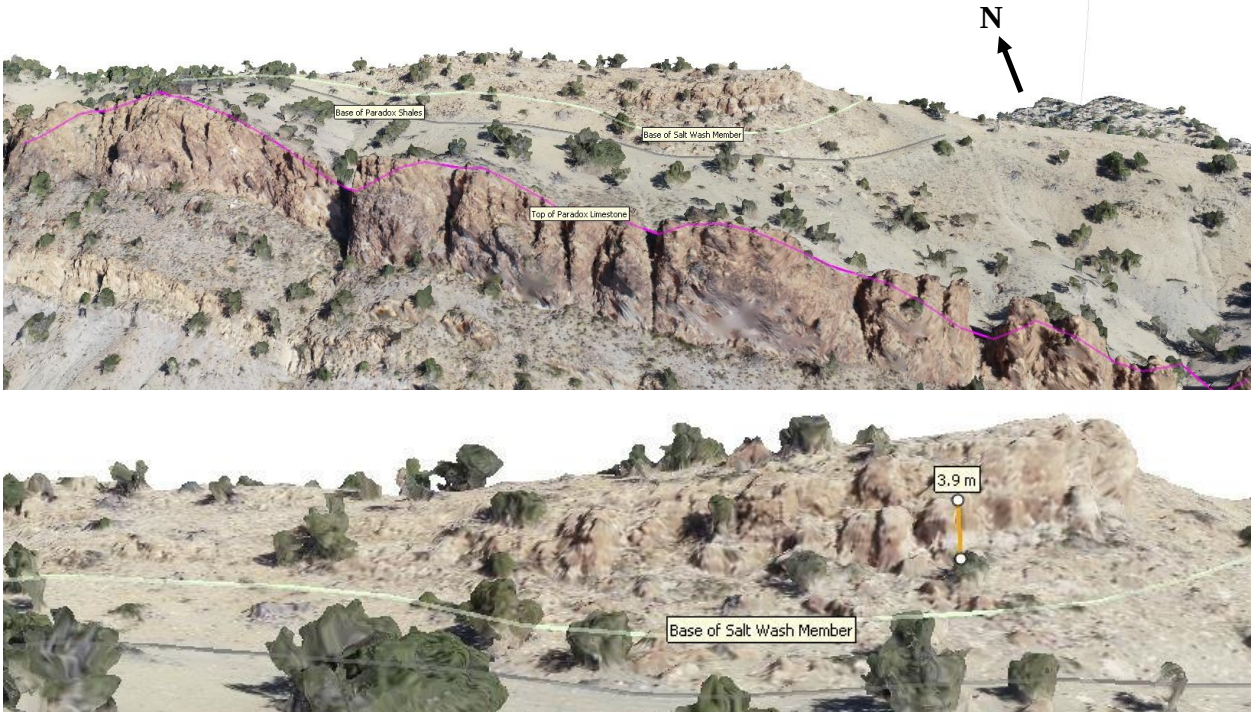

Figure 11: Perspective view of the 3D model of the Paleo Canyon in area A, showing a) the Morrison Formation incising and onlapping onto the underlying Paradox Shales with a gentle slope towards the west. b) Close-up to the Morrison Formation outcrop. Facing N-NE.

The strata in this outcrop are interpreted to form Bailey's stratigraphic unit 3, which is primarily composed of isolated meandering channel deposits. Lateral accretions in the area are indicative of meandering streams and further confirm where we are in that stratigraphy. The Salt

Wash can be traced along the diapir margin and across the salt wall on the detailed maps created for this area (**Figs. 4, 8**). The channels are atypical of this unit and the shales usually intercalated with sandstones are absent. Four stacked channel fills are exposed in the outcrop (**Fig. 12a**), where the lowest channel is exposed only in the southeastern part of the outcrop with a maximum thickness of 5.5 m. Correlation of strata across the hill shows that there is at least 4 m of onlap on the underlying black shales (**Fig. 12a**). The stratigraphic sections show that 89% of the outcrop is composed of sands and 11% is shales or mudstones. The shales are laterally discontinuous and range from 0.5 to 1 m thick.

A 3-D model of area A was made using 195 photographs acquired using a drone. The model was then created using Metashape software and Illustrator for perspective view annotations. The model was created from a point cloud with 68,141,927 points. A DEM and orthomosaic were created using the imagery with 6 cm/pix and 3 cm/pix resolution respectively. Strata were mapped in three dimensions in metashape to better illustrate the geometries within the Salt Wash Member as it onlapped the black shales of the Paradox Formation and the Honaker Trail megaflap. **Figures 10** and **11** show two different views of this outcrop.

The lowest channel (**Unit 1, Fig. 12b**) is mainly made up of fine grained, well sorted, sub-angular, ripple cross-stratified, light tan to white sandstones with 1 mm to 1 cm thick beds and internal scour marks. Lateral accretion sequences are also evident at its base, which are indicative of meandering streams. The second oldest channel (**Unit 2, Fig. 12b**) is composed of medium grained, moderately sorted, sub-angular, yellow to tan sandstones with 20 cm thick and 25 cm long trough cross beds. The second to last channel (**Unit 3, Fig. 12b**) contains coarse grained, moderately sorted, sub-angular to sub-rounded sandstones with 5-15 cm thick tabular beds and a 5 cm thick lag at the base. Lastly, the highest channel (**Unit 4, Fig. 12b**), is primarily composed

of medium to coarse grained, moderately sorted, sub-angular sandstones with internally scoured beds, 30 cm thick trough crossbeds, and internally cemented clay striations.

Black and green shale chips are found in the lowest channel strata (blue and pink in **Fig. 12**) of the Morrison Formation, indicating that the underlying shale was being eroded during the deposition of the Morrison (**Fig. 13**). Thus, the Morrison Formation is in place and was not faulted into its current location. Also, the chips indicate that the contact is not a salt weld that could have formed the contact due to salt dissolution. Therefore, the Morrison strata were deposited on the shales and not on diapir caprock and then later emplaced through dissolution. This outcrop is interpreted as the eroded base of a paleo-canyon incised into the megaflap strata, which must have formed a topographic high at the time. This interpretation is based on the shale chips found within the basal strata of the Morrison Formation (**Fig. 13**) and the stratigraphic correlations showing the 4 m incision by the four channels into the underlying strata. The 3-D model confirmed this interpretation, with the lowest channel fill 4 m below the highest shale in a direction normal to bedding (**Fig. 11b**)

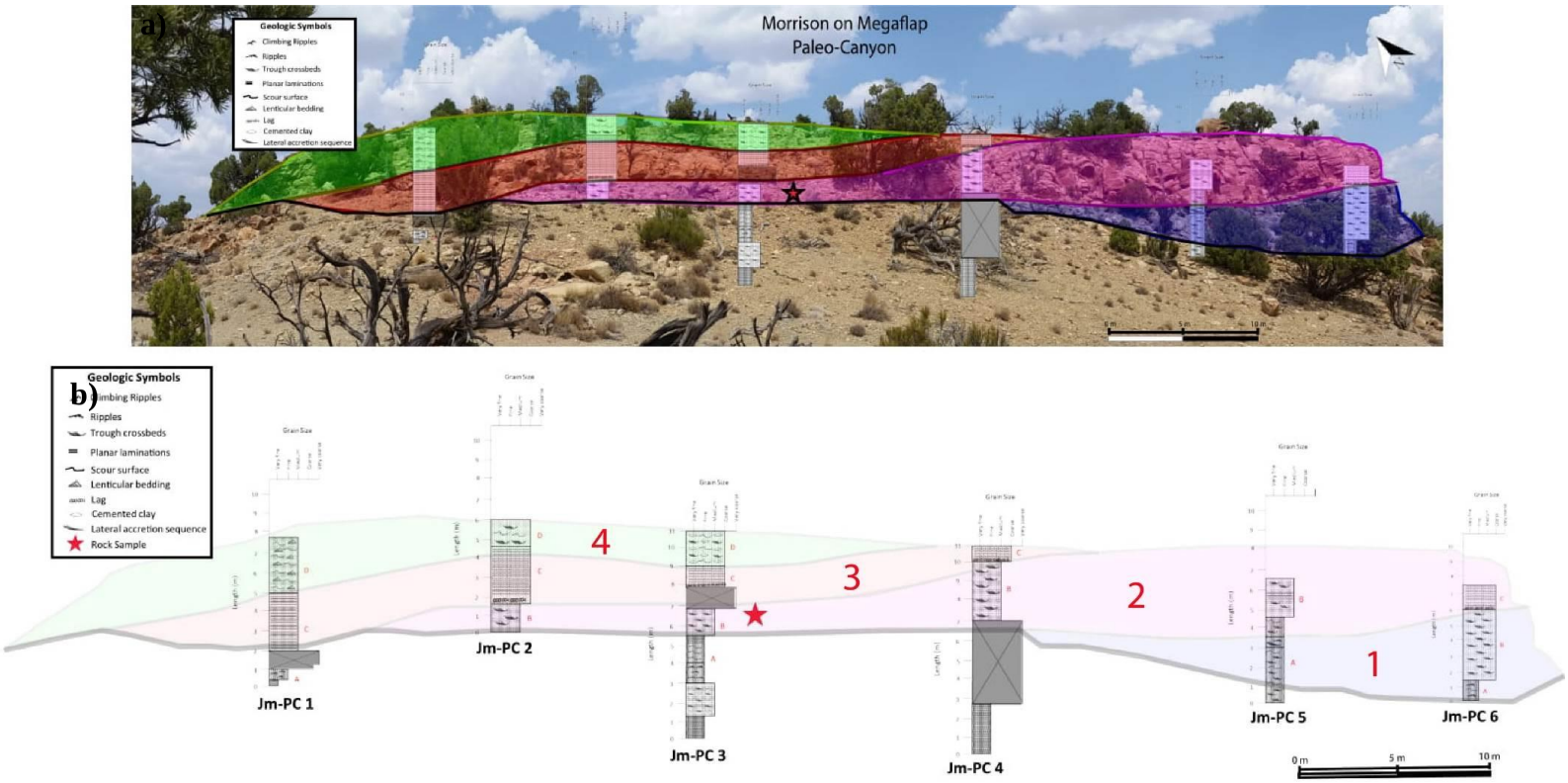

Figure 12: Stratigraphic correlation between 6 measured sections in area A, the Paleo Canyon, showing a) the different channels of the Morrison Formation (green, red, pink, blue) incising and onlapping onto the underlying Paradox Shales and b) a close-up of the stratigraphy within these measured sections (Jm-PC 1 through 6). The red star represents the location where rock sample MSw-A was collected.

Figure 13: Green-black shale chip found within the basal units of the Morrison Formation, which are the result of erosion from the Paradox Shale.

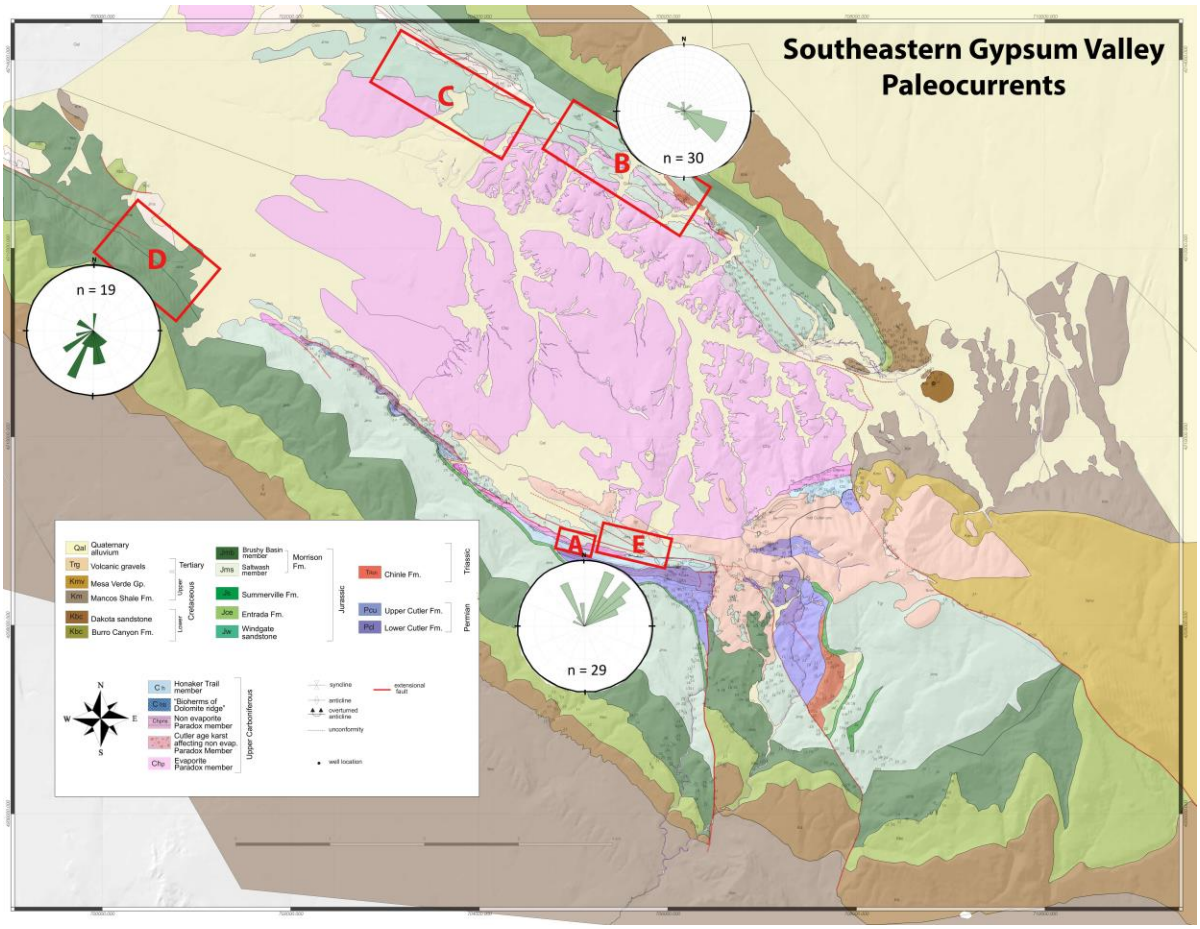

Figure 14: Geologic map of the southernmost end of the Gypsum Valley salt wall in Colorado. Map shows the rose diagrams created from paleocurrent measurements taken along trough cross beds within the Salt Wash Member of the Morrison Formation in study areas A, B and D. Area A shows 28 measurements which indicate a mean flow direction of 25.6° NE. Area B shows a mean flow direction to the SE from 30 measurements. Lastly, in area D, 19 measurements show that the mean flow direction is towards 199.6° SW.

Paleocurrent data collected in area A (**Fig. 14**) indicate that the meandering streams that deposited the Morrison Formation were flowing primarily to the northeast into the diapir, which therefore must have been lower than the Disappointment minibasin to the south during Morrison deposition. This allowed for the erosion of the diapir and Honaker Trail megaflap by the first channels that flowed across it. Overall, the rose diagram created in area A from the gathered 28 measurements taken along trough cross beds within the Salt Wash Member of the Morrison Formation, indicate a mean flow direction of 026°.

Area B

Area B covers a 1 km^2 region that is located on the northeastern rim of the salt wall at Big Gypsum Valley (**Fig. 8**). The area exposes folded Morrison Salt Wash strata resting on Paradox gypsum (**Fig. 15**). This area lies at the base of an escarpment composed of a prominent cliff-formed unit within stratigraphic unit 4 of the Salt Wash Member. This is overlain by a slope composed of the green conglomeratic Brushy Basin Member of the Morrison Formation, the Burrow Canyon Formation, and the cliff-forming Dakota Sandstone. These upper units dip to the northeast towards the Dry Creek minibasin at an average 16° (**Fig. 7**).

A 3-D model of area B was created on Metashape using 823 photographs acquired by drone (**Fig. 15**). The resulting point cloud, composed of 89,014,450 points, was then used to create a DEM and orthomosaic image of the study area to be used for field mapping. These were of a resolution of 5.37 cm/pix and 2.69 cm/pix respectively.

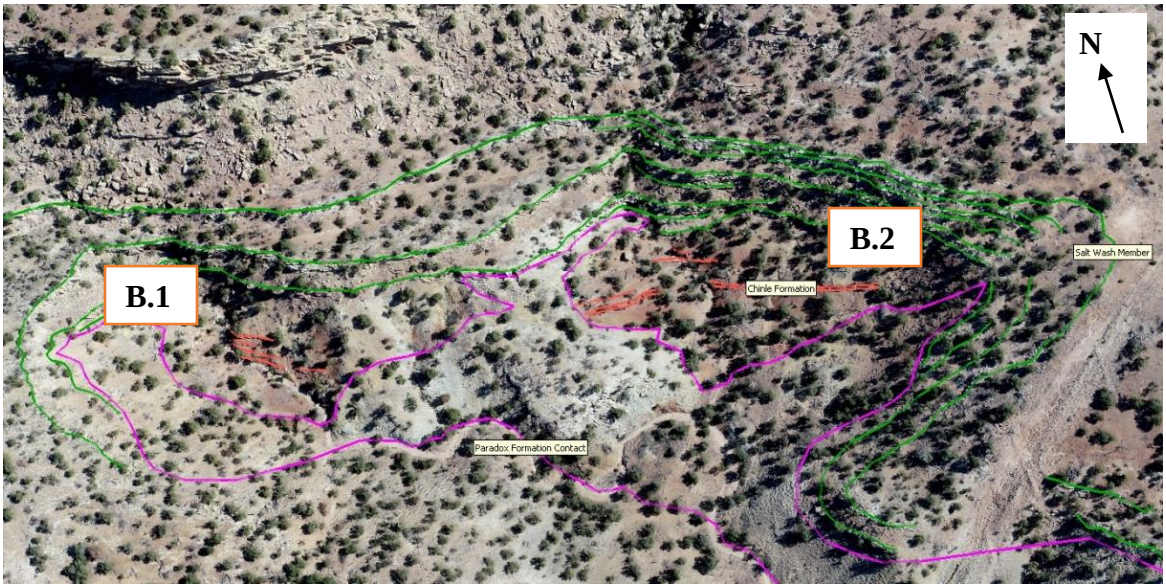

Figure 15: Perspective view of 3D model of Area B looking N-NE. Green lines show bedding traces in the folded Salt Wash Member overlaying the Paradox Formation (to of Paradox shown in pink) and Chinle Formation (bedding traces shown in red). Sites B.1 and B.2 are also shown above.

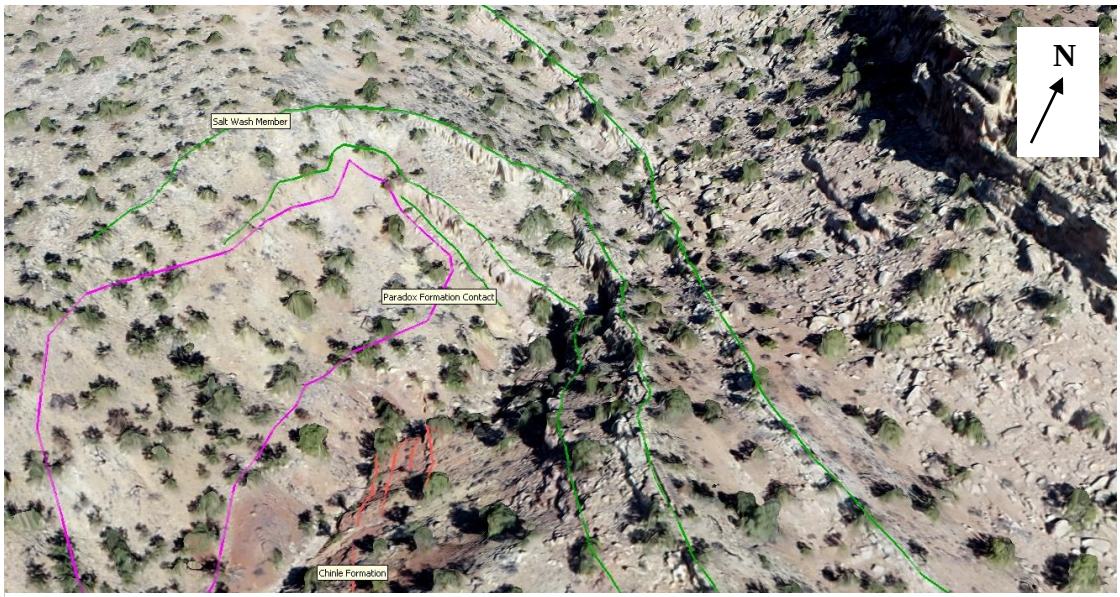

Figure 16: Perspective view of 3D model of Site B.1 looking N-NE. Green lines show bedding traces of the Salt Wash Member folding into an anticline and overlaying the Paradox Formation (top of Paradox shown in pink), and the vertically dipping Chinle Formation (bedding traces shown in red).

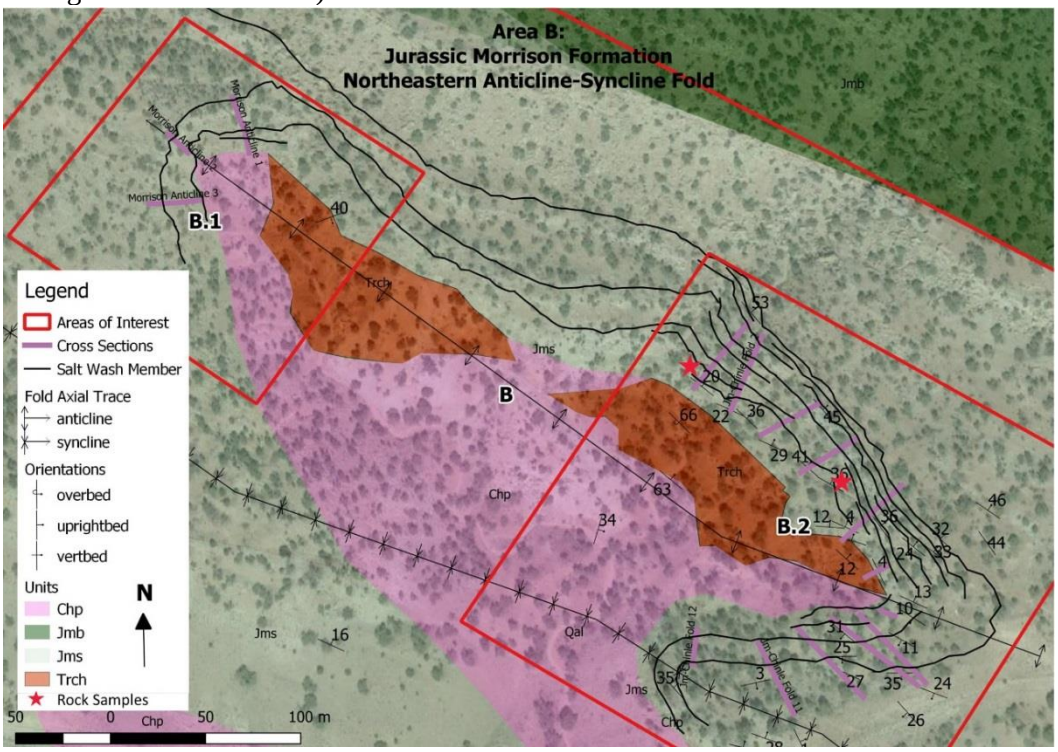

Figure 17: Stratigraphic sections examined in Area B shown as purple lines, which are subdivided into sites B.1 and B.2. Basemap is an orthomosaic image acquired from a 3D model. The red stars show the locations for rock samples MSw-B1 and MSw-B2.

Site B.1 exposes Bailey's stratigraphic unit 3 of the Salt Wash Member folding into an anticline, where the northern limb of the fold overlies Chinle Fm. strata dipping at 66°-80° NE in

angular unconformity (**Fig. 16**). Three stratigraphic sections were measured on this site and correlated to better illustrate the internal geometries of the Morrison Formation (**Fig. 17**). The Salt Wash strata extend for 595 meters to the NE-SW perpendicular to the diapir margin and 480 meters into the diapir on the salt. On the northeastern limb, strata dip at 40° into the Dry Creek Minibasin (**Fig. 17**). On the southwestern limb of the anticline, strata dip between 20-35° into the diapir. Strata can be traced across the diapir margin unfaulted over the crest of the anticline before pinching out against Paradox gypsum. However, underlying strata of the Salt Wash can be observed to onlap more steeply dipping strata of the Chinle Formation.

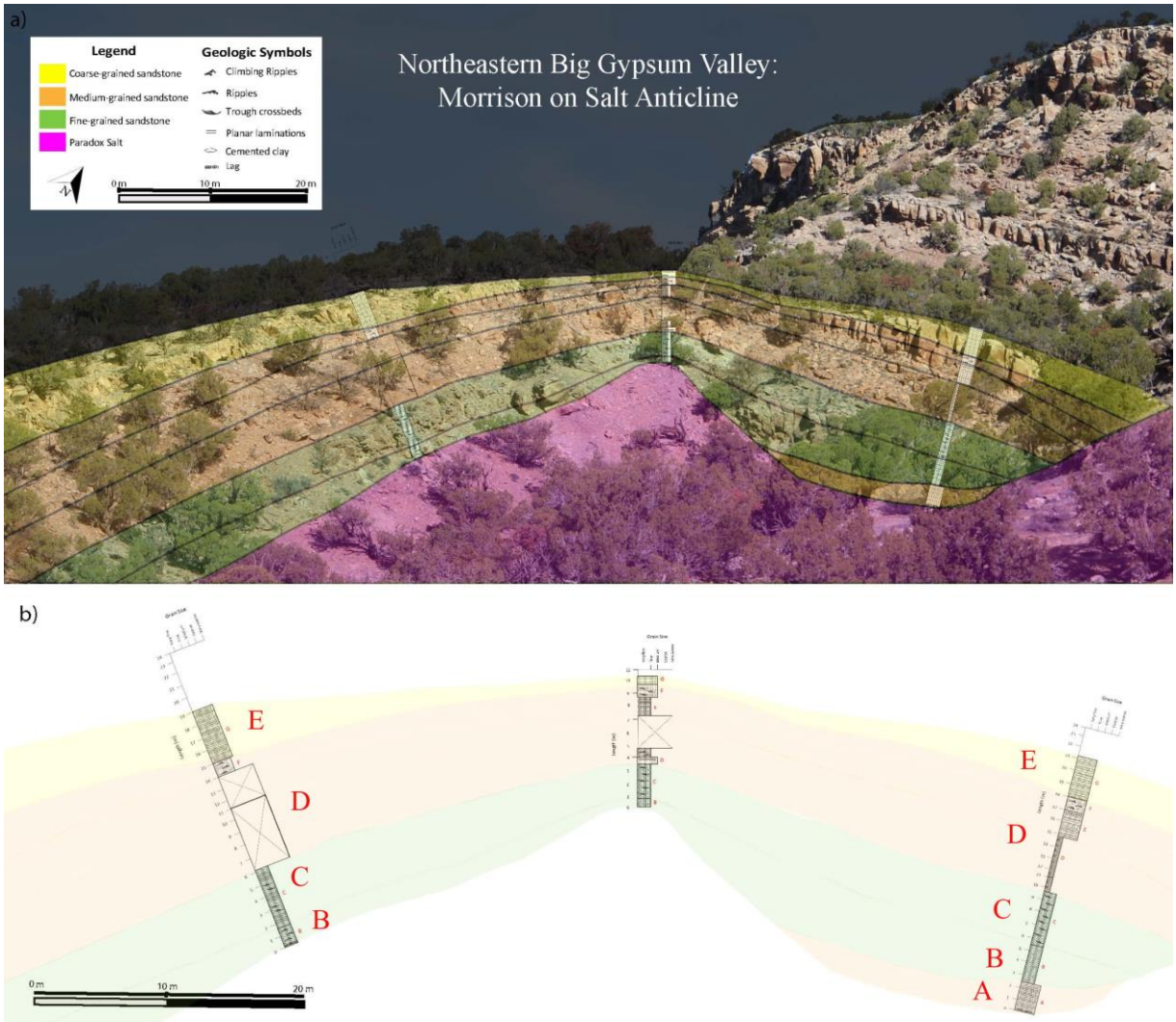

Figure 18: Stratigraphic correlation of three measured sections in site B.1 of Area B, where the Salt Wash Member is folded into an anticline and onlaps the Paradox Formation (pink). a) Shows the channel distribution and b) is a close-up of the individual measured sections.

The stratigraphic sections in site B.1 show that the Salt Wash is composed entirely of sandstone channels that pinch out and onlap the Paradox gypsum (**Fig. 18a**). Remnants of the muds and shales that are common in this unit can be seen at the base of unit beds. The bases of the measured sections were taken at the first well-exposed outcrop of Morrison Formation onlapping the salt and the tops were marked by the last outcrops along the gully before reaching the cliff-forming section of the Salt Wash Member (unit 4). This allowed us to properly correlate units and mark individual bed changes within the anticline. Measured sections vary in thickness from 10 m on the anticline axis to approximately 21 m on the limbs, showing a 52% lateral increase in thickness (**Fig. 18a**).

The individual channels within the Salt Wash Member thicken away from the anticline's axis with a lateral change of 3 m (**Fig. 18b**). The basal channel (**Unit B, Fig. 18b**) on the southwestern limb of the anticline is composed of fine-grained, ripple cross-stratified muddy purple sandstone with an eroded base and lag. Up section, unit C is a trough cross-stratified sandstone with interbedded 10 cm thick tabular beds (**Fig. 18b**). The centermost unit (**Unit D, Fig. 18b**), is composed of a medium to fine-grained, well-rounded, well-sorted, sandstone with 5 cm thick tabular beds and 2 mm thick laminations. Beds within unit D alternate from medium grained, well-sorted, sub-rounded, ripple cross-stratified sandstones at the limbs of the anticline to medium grained, 40 cm thick, 70 cm long trough cross-bedded sandstone at the fold axis. Lastly, the upmost channel (**Unit E, Fig. 18b**), contains a coarse-grained, cliff-forming sandstone with 1-2 cm thick laminations. These same units can be observed on the northeastern limb of the anticline, but with an additional channel at the base, unit A. Unit A is composed of a well-rounded, medium to fine-grained, white sandstone with 5-10 mm thick lenticular bedding and an eroded base with gravel lags.

The same anticline in site B.1 crops out in site B.2. However, a syncline is exposed to the southeast, creating an asymmetrical anticline-syncline fold couple whose axial plane runs parallel to the salt diapir's margin (**Fig. 17**). The syncline can be traced to where it is buried beneath Quaternary alluvium, and is inferred to be buried in site B.1. The strata in this site can be correlated across the gully to units D and E in site B.1 (**Figs. 15, 18b**). In the core of the anticline, vertically-dipping Chinle Formation strata underlie an angular unconformity beneath the Salt Wash Member (**Fig. 19, 21**). To the southeast, the Chinle Formation overlies the Paradox Formation caprock, which is exposed in scattered outcrops of gypsum and dolomite. Twelve stratigraphic sections were measured and correlated in site B.2 to illustrate geometries and changes in bed thickness in the folds (**Fig. 17**). The Salt Wash crops out for approximately 645 meters NE-SW perpendicular to the diapir margin and 504 meters into the diapir on the salt. Strata dip 40° northeast into the Dry Creek Minibasin before folding over an anticline and then dip at 28° southwest into a syncline (**Figs. 15, 17**). Strata can be traced along the diapir margin with no faulting along the crests of the folds.

Measured sections at site B.2 contain an average of 67% sandstones and 38% shales (**Fig. 19a**). Strat sections vary in thickness from 11 m on the anticline axis to 33 m on the syncline axis. Individual units thin onto the anticline and thicken into the syncline with a lateral change of about 4-5 m (**Fig. 19b**). Beginning on the northeastern limb of the anticline, the base of the Salt Wash Member is a series of upward coarsening sequences (**Fig. 19b**). The base unit (**Unit 1, Fig. 19b**) consists of fine-grained sandstones with 1 cm thick climbing ripples, extending for 35 m towards the anticline axis before pinching out against the underlying Chinle Formation (**Fig. 19a**). The next channel up-section (**Unit 2, Fig. 19b**) is composed of coarse grained, trough cross-stratified sandstone with a maximum thickness of 3 m on the northwest and a minimum of 1 m before

onlaping against the Chinle Formation (**Fig. 19a**). Farther up-section, units alternate from poorly exposed green shales (Unit 3) to fine-medium grained sandstones with 1 cm thick tabular beds (Unit 4) to trough cross-stratified coarse-grained sandstones (Unit 5) (**Fig. 19b**). On the anticline axis, a 0.5 m thick coarse-grained sandstone (Unit 5) crops out above a 10 m thick, poorly exposed shale layer (**Fig. 19b**). To the southeast, the Salt Wash forms a syncline with a maximum thickness of 30 m with upward-coarsening channel deposits. At the base, a very fine grained, well-rounded, well-sorted, oxidized white sandstone (Unit 1) with 40-50 mm thick tabular beds extends for 15 meters north-south and pinches out against Paradox gypsum. Unit 3 is similar to unit 1 and overlies a 5 m thick shale unit (Unit 2) (**Fig. 19b**). Unit 3 laterally extends at least 10 m more than the base unit in the north-south direction (**Fig. 19b**). Beds dip a max of 35° on both sides of the fold axis (**Fig. 17**). Up-section along the syncline, units alternate from fine-medium grained sandstones with tabular beds and cemented clay to green-black shales to coarse grained, trough cross-stratified sandstone. Like area A, the basal units within the Salt Wash Member in site B.1 contain diapir derived clasts, including Paradox dolomite and mud chips (**Fig. 20**).

A SW-NE cross section was made across area B to better illustrate the geometries of strata below the surface (**Figs. 4, 21**). Like in the stratigraphic correlations, the model shows that the Morrison Formation is thinning on the flanks of the syncline. Beds sit on salt along the diapir margin to form a salt shoulder. The change in bed thickness is consistent with the previous observations and further emphasizes that deformation occurred syndepositionally.

Paleocurrent data gathered from trough cross-beds within the Salt Wash in area B show that the mean flow direction is to the southeast, parallel to the fold axis (**Fig. 14**). This indicates that the salt tectonism is probably directing flow as channels are flowing parallel to the fold axes and the diapir margin.

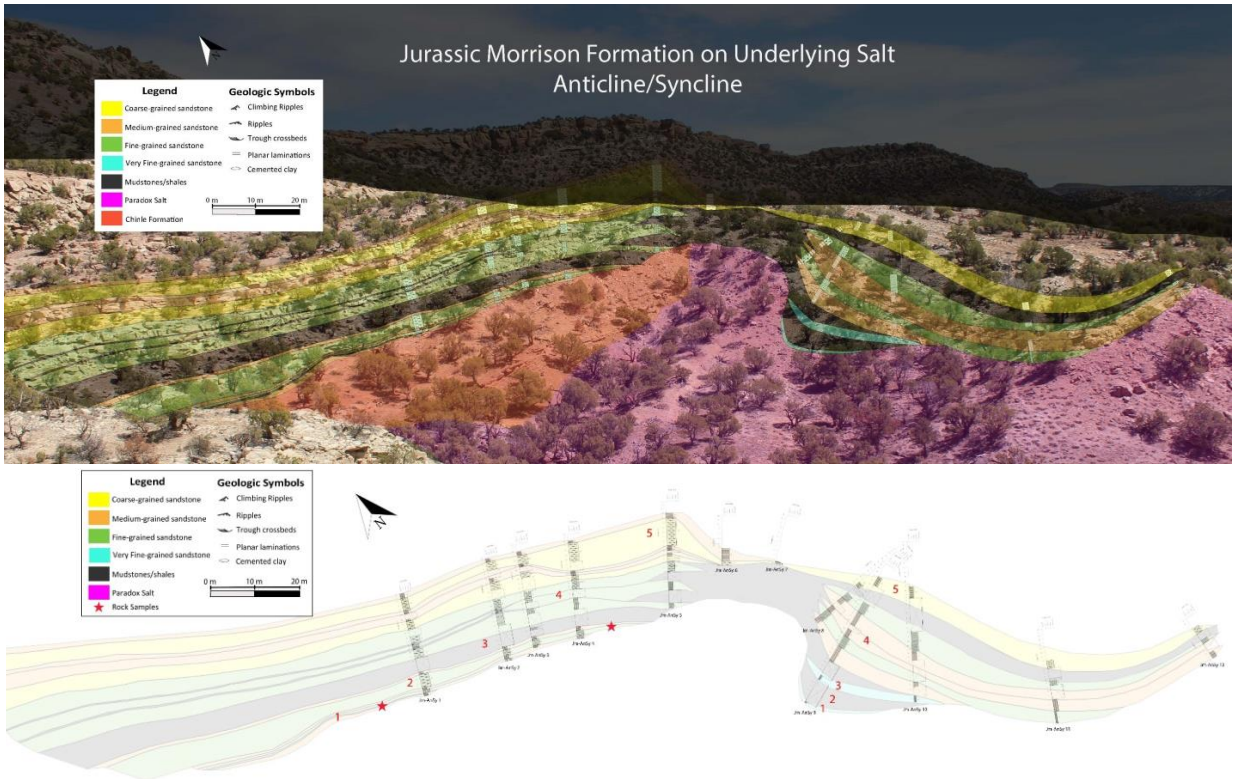

Figure 19: Stratigraphic correlation of twelve measured sections in site B.2 of Area B, where the Salt Wash Member is folded into an anticline-syncline pair and onlaps the Paradox Formation (pink) and Chinle Formation. a) Shows the channel distribution and b) is a close-up of the individual measured sections. The red stars show the locations for rock samples MSw-B1 and MSw-B2.

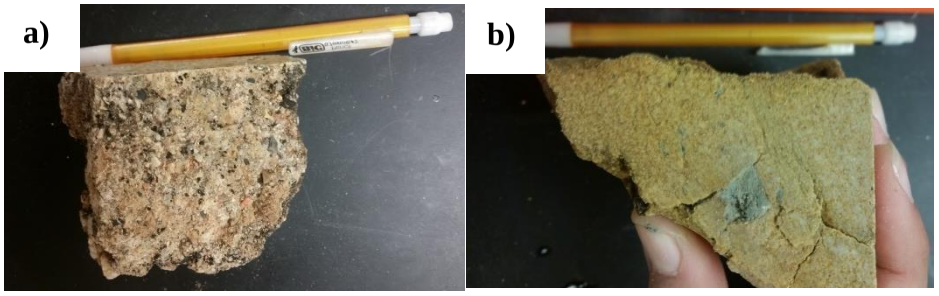

Figure 20: Samples collected from the base unit of the Salt Wash Member at site B.2, where a) shows Paradox dolomite clasts and b) contains diapir-derived mud chip.

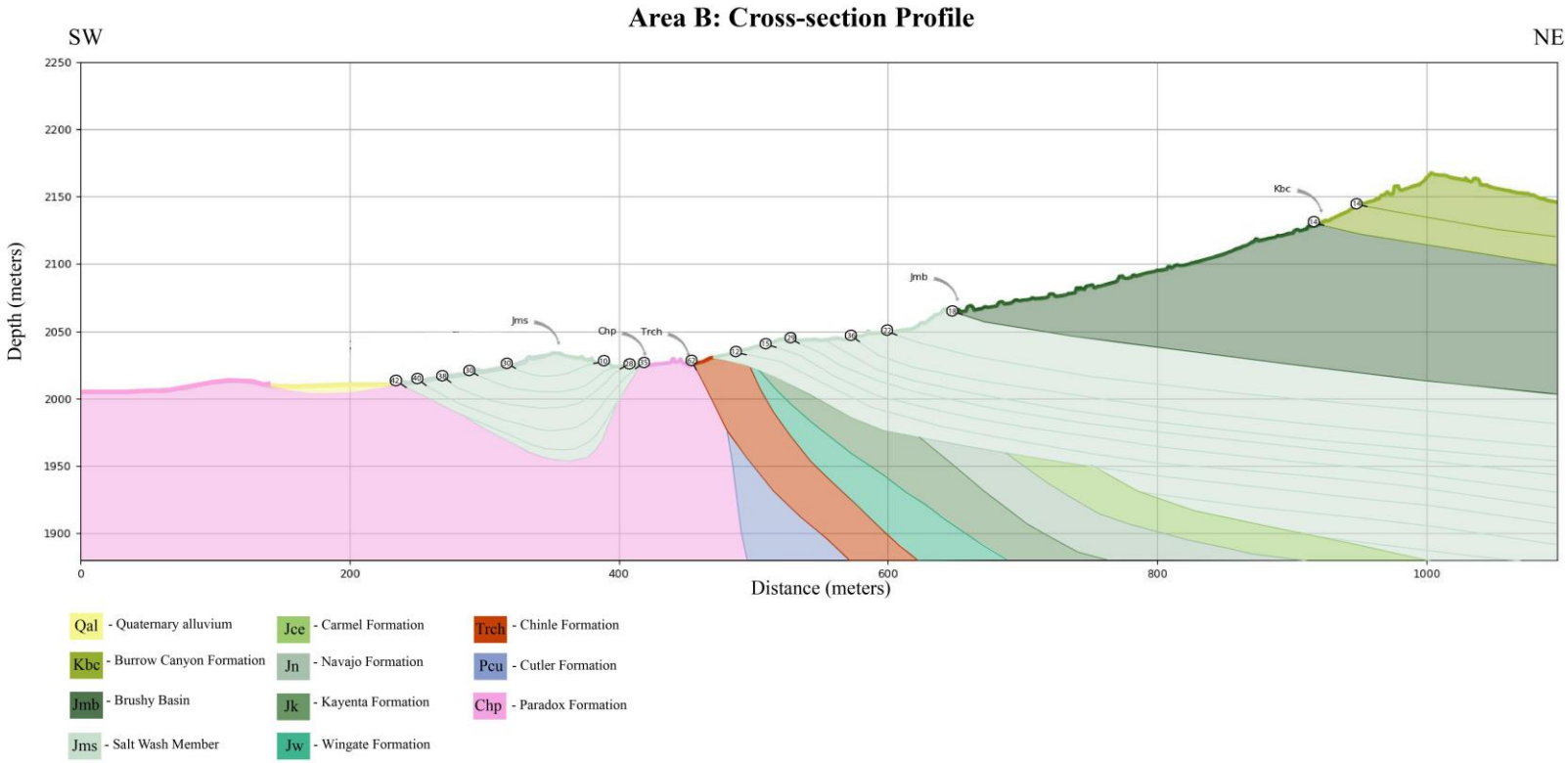

Figure 21: SW-NE cross sectional view of the Morrison Formation folding into an anticline-syncline pair on the northeastern margin of the salt diapir in Big Gypsum Valley, Colorado (Fig. 4). The Salt Wash Member of the Morrison Formation is folded and onlapping Paradox caprock, forming a salt shoulder. Beds within the formation thin along the anticline axis and thicken on syncline axis before pinching out against the salt.

Area C

Area C is located on the northeastern flank of the salt wall, a 1.3 km^2 region where the Salt Wash Member of the Morrison Formation forms a syncline-anticline-syncline fold system that onlaps Paradox diapir caprock (**Figs. 3, 4, 22**). The Salt Wash is exposed as a series of scattered outcrops that are predominantly composed of isolated meandering channel deposits. Between the outcrops, the Salt Wash is covered by soil and alluvium (**Fig. 22**). The Salt Wash extends for a maximum 1,168 meters to the northeast and southwest perpendicular to the diapir margin and 660 meters into the diapir on the salt, where folding occurs (**Fig. 22**). Northeast of the folds, the Chinle Formation is exposed at the surface for 233 m perpendicular to the diapir margin (**Fig. 22**). Chinle strata dip an average 80° northeast towards the Dry Creek Minibasin (**Figs. 4, 22**). From the Chinle Formation, the Salt Wash extends another 293 m away from the diapir to the northeast before the upper member of the Morrison Formation, the Brushy Basin, is exposed at the surface.

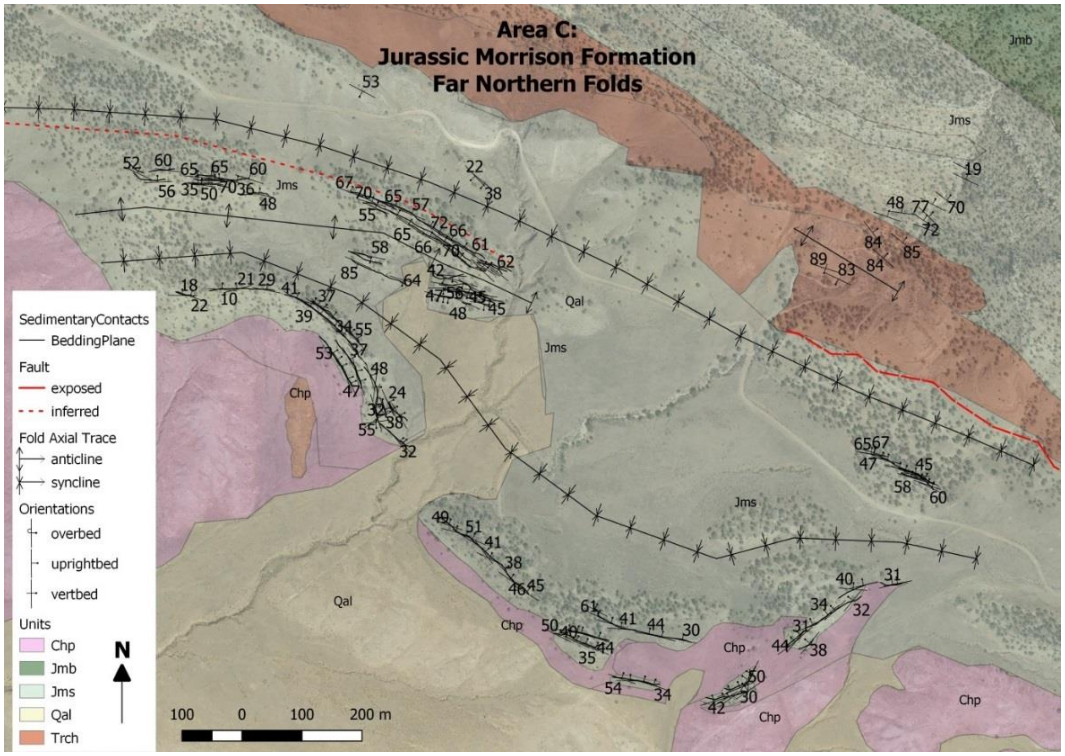

Figure 22: Geologic map of area C, located on the northeastern flank of the salt wall. The Morrison Formation is exposed as scattered outcrops and forms a tight syncline-anticline-syncline fold system onlapping salt. Basemap is an orthomosaic image acquired from 3D model.

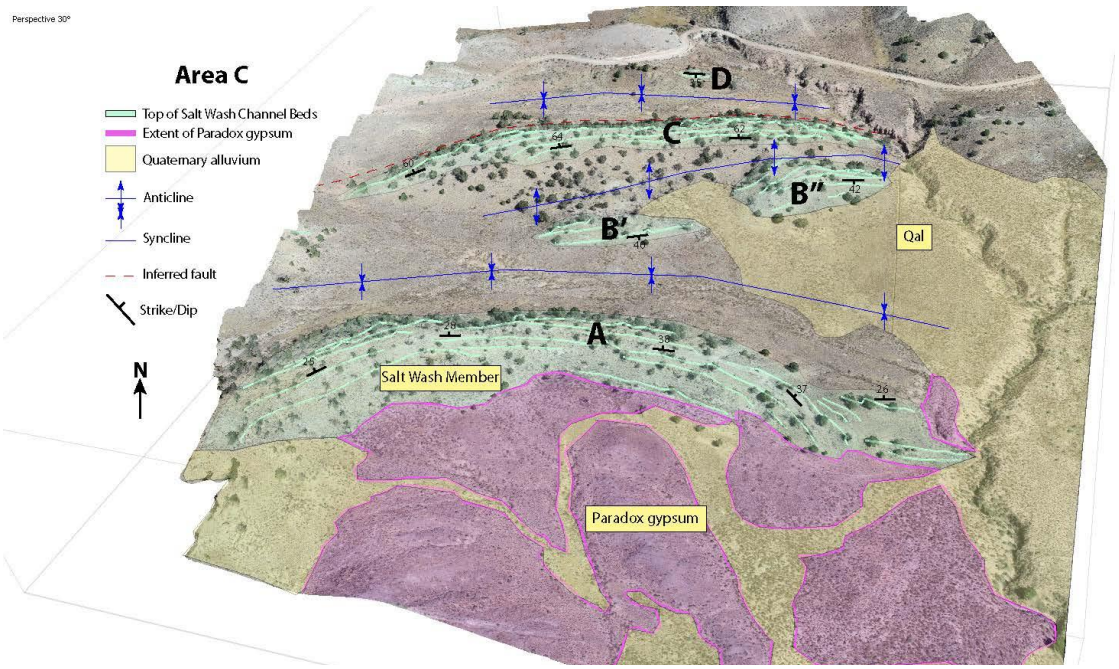

Figure 23: Perspective view of 3-D model for area C looking north at a near vertical angle. Here, the Morrison Formation forms a syncline-anticline-syncline fold system on the northeastern margin of the salt wall. The green lines mark the top of channel beds within the Salt Wash and pink shading shows Paradox caprock and yellow shading is Quaternary alluvium.

A 3-D model of the northwestern section of area C was made using drone photogrammetry, where the green lines show the top of Salt Wash channels (**Fig. 23**). Pink shading shows Paradox caprock outcrop and the yellow shading is Quaternary alluvium (**Fig. 23**). The model was created from 682 photographs, resulting in a point cloud with 93,052,476 points. A DEM and orthomosaic image were created from this model with resolutions of 5.37 cm/pix and 2.69 cm/pix respectively. The orthomosaic image was used as the basemap for the mapping in area C. In area A of the model, the Salt Wash crops out parallel to the salt wall margin for 1,627 meters east to west with dips between 25-50° NE (**Figs. 22, 23**). Individual channels extend for a maximum of 200 m and a minimum of 20 m before pinching out against the salt or neighboring channel beds (**Fig. 22**). The next outcrop (B) is located 100 m northeast from the previous as two separate segments, B' and B", extending for 113 m east to west each with dips ranging from 40-65° SW. Outcrops A and B lie on opposite limbs of the syncline that runs parallel to the salt wall. Channels within outcrop B

pinch out on the east and west ends of the hills and against neighboring channel beds. Outcrop C is located 23 meters from the previous, extending for 640 meters east to west. Units in outcrop C have a dip between 47-60° NE, marking the presence of a tight anticline between outcrops B and C. Lastly, outcrop D is located 82 meters further northeast, extending for 45 meters east to west and dipping gently at an average dip of 30° SW. The change in dip between outcrops C and D mark the presence of a syncline. A normal fault is inferred to be present between these two outcrops, extending for 380 meters east to west in order to account for the drastic change in dip between outcrops C and D.

Area D

Area D is located on the southwestern flank of the salt wall in Big Gypsum Valley (**Figs. 3, 4, 8, 24**). It covers a 0.782 km^2 area where the upper unit of the Morrison Formation, the Brushy Basin, folds into a syncline-anticline pair and the Paradox Formation is covered by Quaternary alluvium adjacent to the outcrops (**Fig. 24**). Along the salt margin, the Salt Wash Member extends 175 meters to the southwest before being buried beneath the Brushy Basin. The Brushy Basin extends for a total of 1259 meters SW-NE before being overlain by the Cretaceous Burrow Canyon to the southwest (**Fig. 4**).

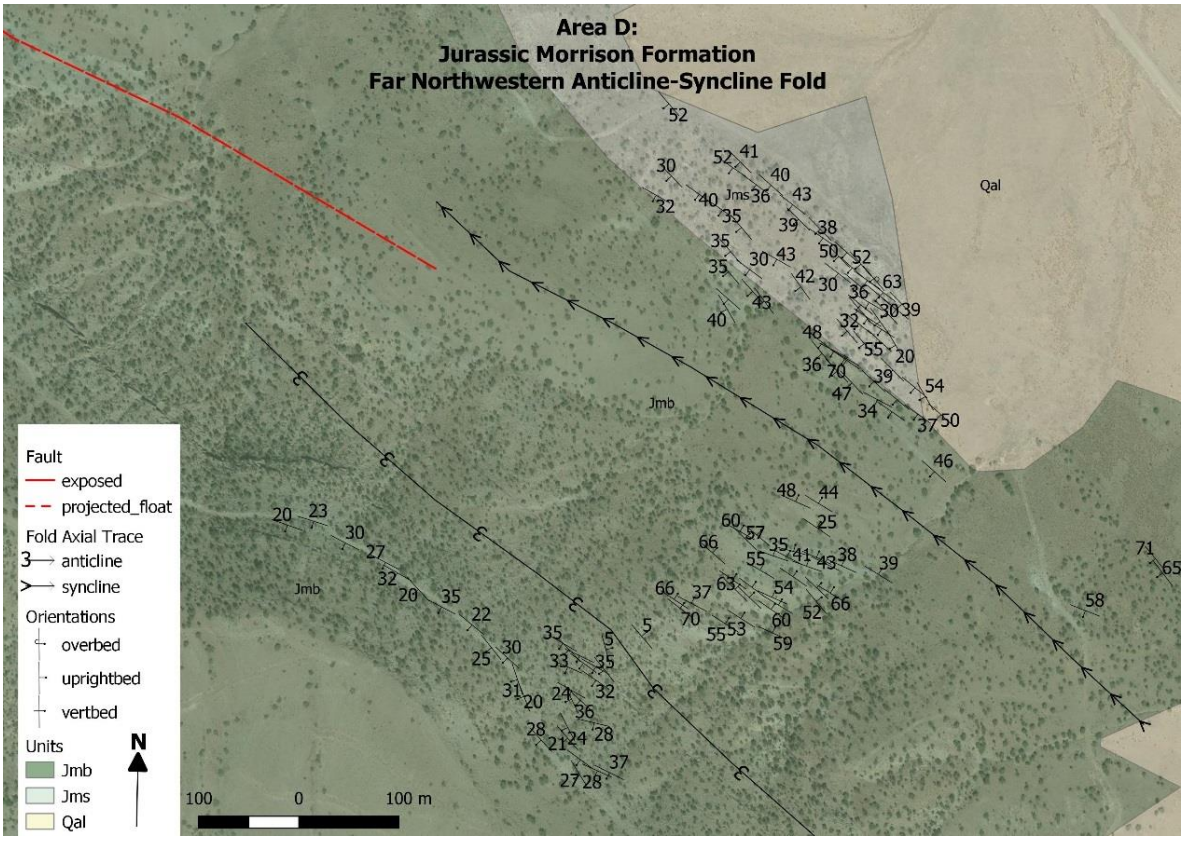

Figure 24: Geologic map of area D, located on the northwestern flank of the salt wall in Big Gypsum Valley, where the Brushy Basin folds into a syncline-anticline pair. Basemap is an orthomosaic image acquired from 3-D model (Fig. 24).

A 3-D model of area D was created with the use of 175 images acquired by a drone (**Fig. 25**). These images were processed in Metashape, generating a point cloud with a total of 65,270,782 points. This point cloud was then used to build a DEM and orthomosaic image of the area with 5.59 cm/ pix and 2.79 cm/pix resolutions respectively. The orthomosaic image was then used as a basemap for mapping of this area.

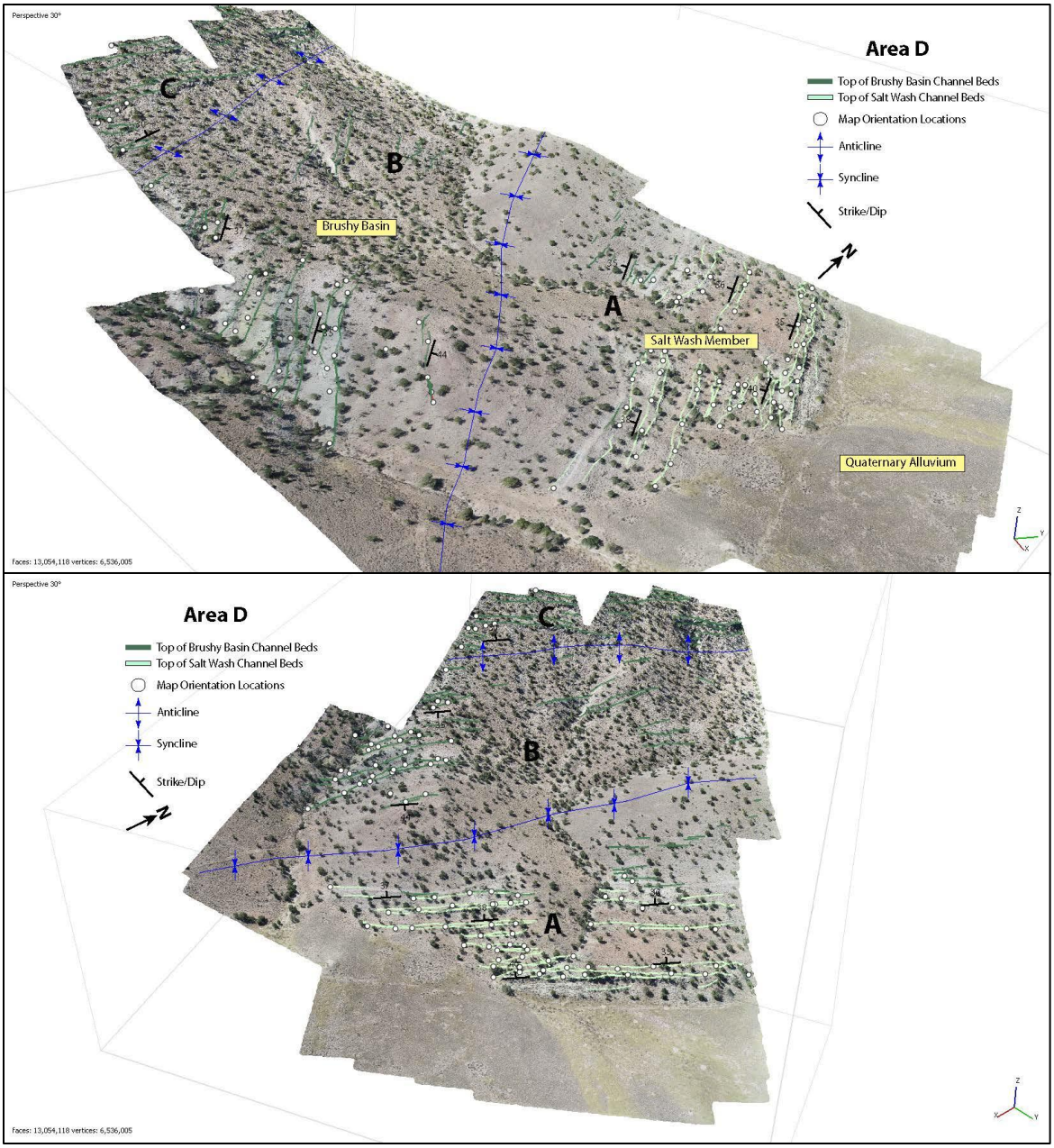

Figure 25: Two perspective views of the 3-D model of area D, located on the northwestern margin of the salt wall in Big Gypsum Valley, CO. Upper figure is looking N-NW at a relatively low angle whereas the lower figure is looking west at a moderate angle (note reference axis in corners). Areas A and B lie on opposite limbs of a syncline while areas B and C are separated by an anticline. The folding takes place within the upper unit of the Morrison Formation, the Brushy Basin.

There are two folds in area D, as seen in the 3-D model (**Fig. 25**). Closest to the salt wall margin, the northeastern limb of the syncline is composed primarily of laterally stacked meandering channel deposits, which form unit 4 of the Salt Wash Member of Bailey's

classification. Along the syncline axis, the Brushy Basin is seen as poorly exposed, slope-forming green-purple shales, marking the top of the unit 4 of the Salt Wash Member. Stratigraphic units within site A, on the northeastern limb of the syncline, dip on average 40° SW towards the Disappointment minibasin. On the southwestern limb of the syncline (B), tannish-green chert-pebble conglomeratic sandstones of the Brushy Basin dip between 35-55° NE (**Fig. 25, 26**). This unit extends for 258 meters perpendicular to the diapir margin before changing dip direction to the southwest to form an anticline (**Fig. 4**). The southwestern limb of the anticline (C) is composed of trough cross-stratified conglomeratic sandstones of the Brushy Basin, with beds dipping between 20-35° southwest (**Fig. 25, 27, 28**). Throughout area D, beds are commonly poorly exposed and shown as scattered outcrops that pinch out against neighboring beds or Quaternary alluvium (**Fig. 25**).

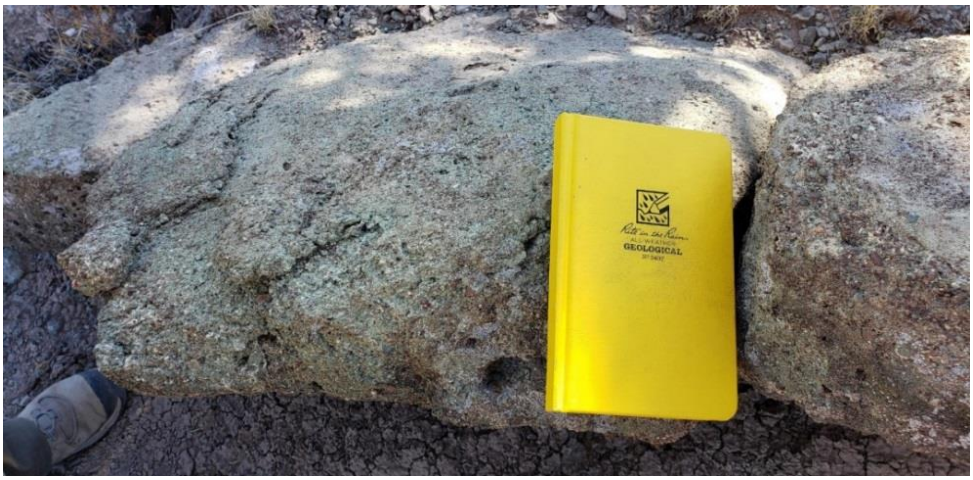

Figure 26: Green, chert-pebble conglomeratic sandstone of the Brushy Basin.

Figure 27: Conglomeratic sandstone to pebble trough cross-stratified sandstone of the Brushy Basin located in area D.

Figure 28: Tan to greenish trough cross-stratified sandstone of the Brushy Basin member of the Morrison Formation in area D.

Paleocurrent data were gathered along trough cross-beds within Brushy Basin sandstones, showing that the mean flow direction is toward 199.6° (southwest) (**Fig. 14**). This indicates that the Disappointment minibasin to the southwest was lower than area D during the deposition of the Brushy Basin.

Area D

Area E is located on the southwestern margin of the salt wall and north of the incised canyon of area A (**Fig. 8, 29**). Here, the Salt Wash Member of the Morrison Formation forms a syncline parallel to the salt margin, where beds onlap salt. The Salt Wash extends for approximately 337 meters northeast to southwest perpendicular to the salt wall, all of which is located on top of salt. North of the fold, beds have a maximum dip of 66° SW closest to the fold

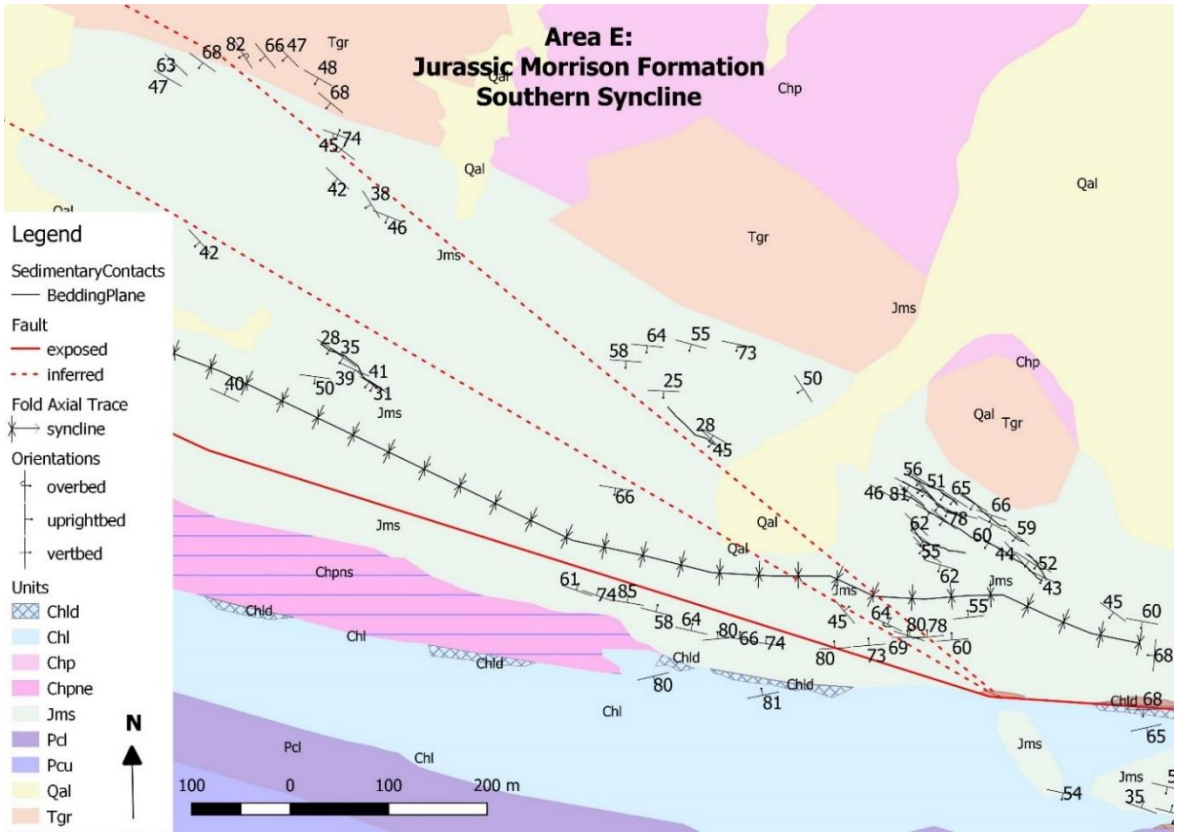

Figure 29: Geologic map of area E, located on the southwestern margin of the Gypsum Valley salt wall and north of area A. The Morrison Formation folds into a syncline and onlaps Paradox gypsum.

axis and become gentler farther northeast. On the southwestern side of the fold, Morrison beds dip between 64-80° NE along a steep slope with scattered outcrops and dense vegetation.

Area E is also characterized by a series of down-to-the-North normal faults that are subparallel to the diapir margin, branching out from the major western radial fault (**Figs. 4, 29**). The southernmost fault can be traced approximately 2.54 km west-east along the steep slope on the southwestern limb of the anticline. The Salt Wash dips a maximum of 80° NE along the fault and then becomes gentler to the northeast before changing dip direction. The other two normal fault diverge from the first and are mainly located on the northeastern limb of the syncline, each extending for approximately 1.83 km northwest-southeast. The northern margin of the Morrison outcrop is largely buried under Tertiary conglomerates (**Fig. 29**).

Morrison beds are difficult to trace along the southern limb of the fold due to the steep slope, poor outcrop exposure, and dense vegetation in the area. However, exposed outcrops on the northern limb of the syncline are found to pinch out against the Paradox caprock. Overall, the Salt Wash in this area is found to form isolated channel deposits divided by shales and quaternary alluvium. This unit is interpreted to be unit 3 of the Salt Wash and can be traced all along the diapir margins, following the same patterns as in areas A-C.

Petrographic Analysis

Three rock samples were gathered from the basal units of the Salt Wash Member of the Morrison Formation in areas A and B, where beds onlap the Paradox Formation. In hand sample, apparent diapir-derived clasts could be seen within these basal sandstone beds (**Fig. 13, 20**). Petrographic thin sections were made from three samples in order to determine whether these clasts originated from the Paradox Formation. A total of 400 points were point counted to estimate the composition of each sample.

Sample MSw-A

The first sample, MSw-A, was collected from unit 1, the basal channel of the Salt Wash Member in area A (**Figs. 4, 9, 12**). This bed forms part of unit 3 of the Salt Wash Member of the Morrison Formation and is located east of stratigraphic section Jm-PC 3, which is composed of a medium grained, trough cross-stratified sandstone. Here, the Morrison Formation incised into the underlying Paradox black shales and Honaker Trail megaflap on the southwestern margin of the salt wall (Deatrick et al.; Rowan et al., 2016; Grisi, 2018). Sample MSw-A is composed of 59.5% grains, 23.25% cement, and 17.25% porosity.

Grains

Of the grain percentage, 64.7% of them are quartz. In sample MSw-A, quartz grains are predominantly sub-rounded to sub-angular, well-sorted and floating in a cemented matrix.

Mudstone and siltstone grains make up 12.2% and 12.6% of the grain percentage respectively and 7.25% and 7.5% of the sample as a whole (**Fig. 30**) (**Table 1**). Mudstone is dark brown in plane polarized light and in reflected light, which is interpreted as a mixture of clay, silt, and organic matter. Clasts are blocky and grains are large enough to image, exhibit first order birefringence in cross-polarized light, and are interpreted as quartz. The mixture gives the sample a salt-and-pepper appearance. Siltstone clasts are light brown in plane polarized light, sub-rounded,

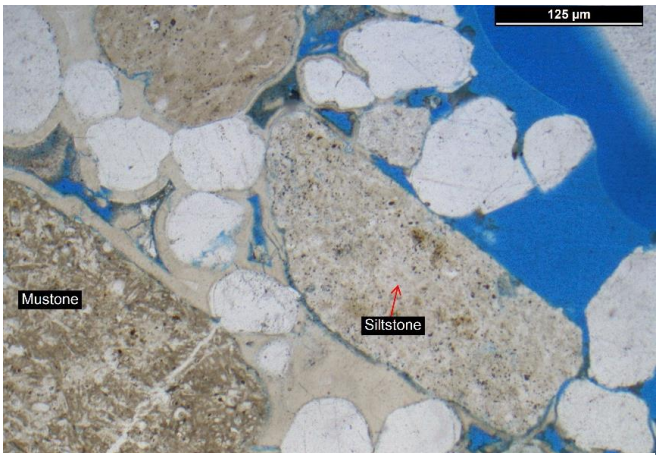

Figure 30*:* Mud and silt grain found in sample MSw-A, collected from the basal strata of the Salt Wash Member in area A in plane polarized light.

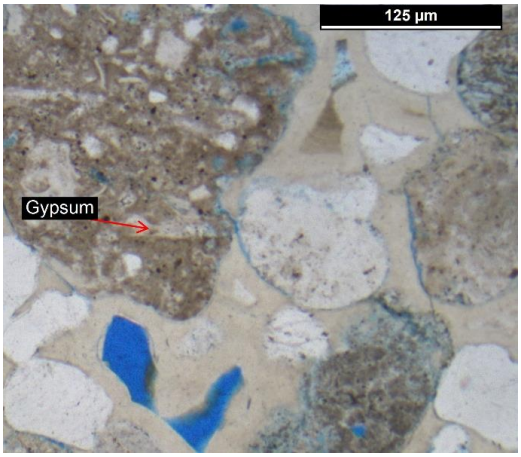

Figure 31: Gypsum grain interbedded in mudstone found in sample MSw-A of area A in plane polarized light.

and exhibits first order birefringence in cross polarized light. They also contain abundant fine grained quartz (**Fig. 30**). Gypsum crystals, make up 1.7% of the percentage of grains and 1% of the sample, have been identified within mudstone grains (**Table 1**). These are colorless in plane polarized light, with a monoclinic habit, and show low relief in cross polarized light (**Fig. 31**).

Chalcedony, a type of microcrystalline quartz, forms 2.1% of the grain percentage in the sample and 1.25% of the sample as a whole (**Table 1**). In plane polarized light, chalcedony is a colorless banded crystal. In cross polarized light, grains appear as yellow-brown grains with zebra banding and a sweeping extinction (**Fig. 32**).

Microcline grains make up 2.9% of the grains and 1.75% of the sample (**Table 1**). These are colorless in plane polarized light and exhibit tartan twinning in cross polarized light (**Fig. 33**).

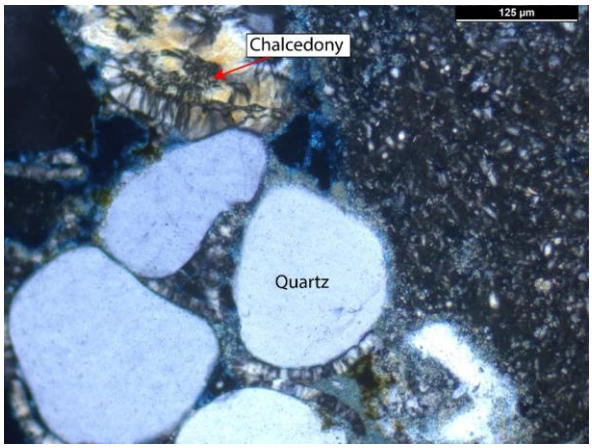

Figure 32: Chalcedony crystal found within sample MSw-A of area A in cross polarized light.

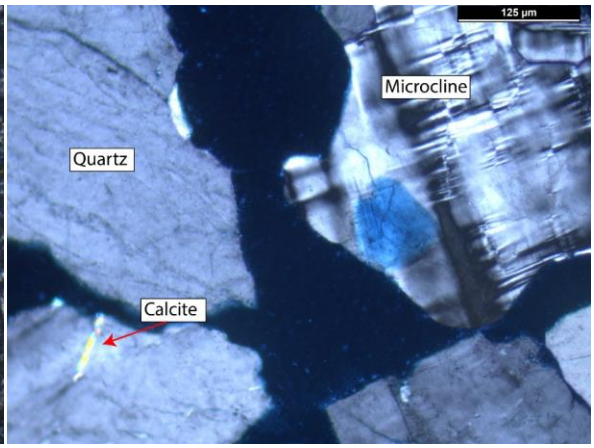

Figure 33: Microcline, quartz and calcite grains from sample MSw-A in cross polarized light.

Calcite and dolomite grains can also be found within sample MSw-A, making up 2.1% and 0.4% of the sample grains respectively (**Table 1**). Calcite and dolomite are both colorless in plane polarized light and exhibit very high birefringence in cross polarized light, showing up as a series of pastel colors (**Fig. 33**). They commonly show lamellar twinning, inclined extinction and perfect rhombohedral cleavage. In sample MSw-A, calcite grains appear as rhombohedral crystals while dolomite grains are fine-grained aggregates.

Other less abundant minerals found within sample MSw-A include chert and hematite. Chert grains make up 0.8% of the grain's percentage and 0.5% of the sample (**Table 1**). Hematite grains make up 0.4% of the grains and 0.25% of the sample (**Table 1**). Hematite is colorless in plane polarized light and brownish-red with high birefringence in cross polarized light. Both hematite and chert are found as small crystals within larger mudstone and siltstone grains in sample MSw-A of the Salt Wash.

Cement

There are four different kinds of cement within sample MSw-A; 1) quartz overgrowth, 2) clay cement, 3) radial quartz, and 4) coarse-grained quartz (**Fig. 34)**. Cements make up 23.25% of the sample (**Table 1**).

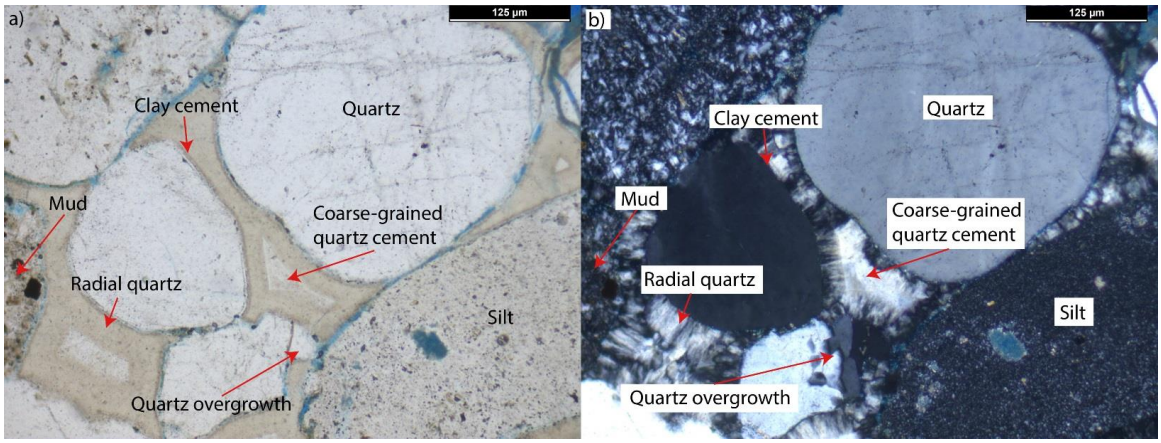

Figure 34*:* Sample MSw -A collected from the Salt Wash Member of the Morrison Formation in area A shown under a) plane polarized light and b) cross polarized light. Image shows the four different stages of cementation found within the sample.

Quartz overgrowth makes up 5.4% of cementation and 1.25% of the sample as a whole (**Table 1**). These areas are defined by the development of quartz cement around detrital grains. Clay cements make up 4.3% of cementation and 1% of the sample (**Table 1**). The clay forms a thin dark halo around larger grains. The largest percentage of cementation is that of radial quartz, making up 76.3% of cementation and 17.75% of the sample (**Table 1**). Radial quartz can be found surrounding most, if not all, grains as a tan border in plane polarized light and a fibrous texture

with low relief in cross polarized light. The last stage of cementation is a coarsely-crystalline quartz, which fills up the remaining pore space. This irregularly shaped quartz cement makes up 14% of cementation and 3.25% of the sample (**Table 1**).

Table 1: Mineral composition of sample MSw-A, collected in area A of the southernmost end of Gypsum Valley, Colorado.

Mineral/Material	**Points (400 Total)**	**Percent Total (%)**	**Type**	**Percent Type (%)**
Quartz	154	38.5		64.7
Mud	29	7.25		12.2
Silt	30	7.5		12.6
Chalcedony	5	1.25		2.1
Chert	2	0.5	59.5 %	0.8
Gypsum	4	1	Grains	1.7
Calcite	5	1.25		2.1
Dolomite	1	0.25		0.4
Hematite	1	0.25		0.4
Microcline	7	1.75		2.9
Quartz overgrowth	5	1.25		5.4
Clay cement	4	1	23.25%	4.3
Radial quartz	71	17.75	Cement	76.3
Coarse quartz cement	13	3.25		14
Solution porosity	25	6.25		36.2
Primary porosity	8	2	17.25% Porosity	11.6
Secondary porosity	36	9		52.2

Porosity

There are three different types of porosity present in sample MSw-A; solution porosity, primary porosity, and secondary porosity (**Fig. 35**). In thin section, a blue dye was used to highlight sample porosity in plane polarized light. Porosity makes up 17.25% of the sample. Solution porosity occurs when grains dissolve due to chemical reactions that take place when they come in contact with water. 36.2% of porosity and 6.25% of the sample is solution porosity (**Table 1**). Primary pores make up 11.6% of porosity and 2% of the sample (**Table 1**). These are identified as smaller pores between grains. On the other hand, secondary pores envelope multiple grains, taking up a larger area. Secondary pores make up 52.2% of porosity and 9% of the sample (**Table 1**).

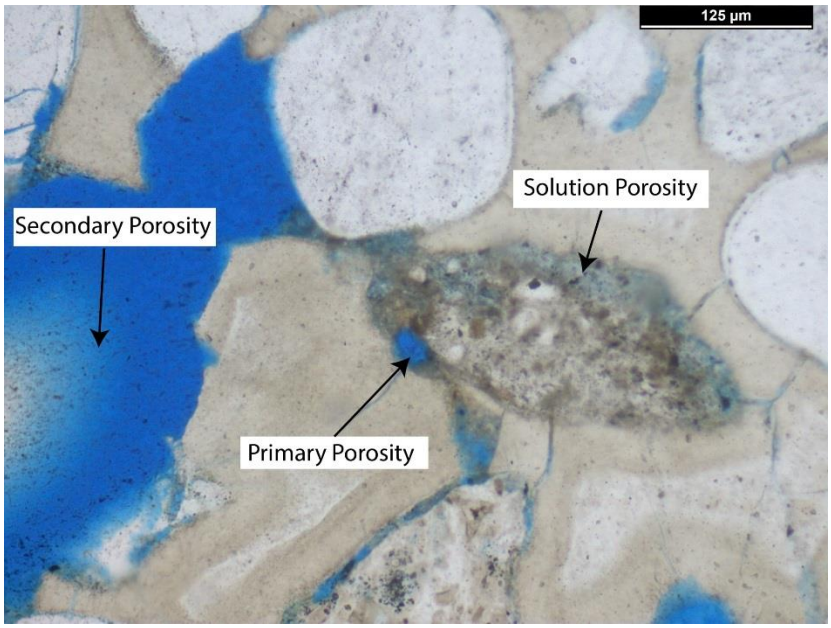

Figure 35: Three types of pores found within sample MSw-A, including solution porosity, primary and secondary porosity.

Samples MSw-B1 and MSw-B2

Samples MSw-B1 and MSw-B2 were collected from units 1 and 2, respectively, of the Salt Wash Member in area B, site B.2 (**Figs. 17, 19**). These units onlap the flanks of the syncline in area B. The strata onlaps Paradox caprock and the near-vertical strata of the Chinle Formation.

Sample MSw-B1 is located on the northeastern end of the anticline limb, while sample MSw-B2 is closer to the anticline axis where beds pinch out against the salt (**Figs. 17, 19**).

MSw-B1: Grains

Sample MSw-B1 is composed of 67.6% grains, 13% cement, and 19.4% porosity (**Table 2**). Of the grain percentage, 82.1% is composed of quartz grains. In this sample, quartz grains are fine-grained, sub-angular and well-sorted (**Fig. 36**). Mudstone and siltstone grains make up 12.1% of the grains and are light to dark brown in plane polarized light. Chalcedony makes up 1% of the grains and microcline makes up 4.7% of the grains.

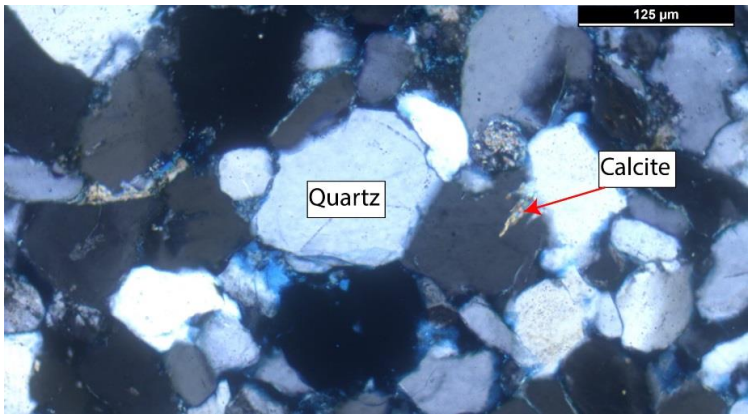

Figure 36: Fine-grained, well sorted, sub-angular quartz grains within sample MSw-B1 in cross polarized light.

MSw-B1: Cement

There are two kinds of cement within sample MSw-B1, calcite and dolomite, making up 13% of the sample. Calcite makes up 3.8% of cementation, filling porosity within quartz grains (**Table 2**) (**Figs. 36, 37**). Dolomite makes up 96.2% of cementation and fills large secondary pore

spaces (**Table 2**) (**Figs. 37, 38**). These cements are easy to identify due to their rhombohedral cleavage and high birefringence in cross polarized light, resulting in pastel colors.

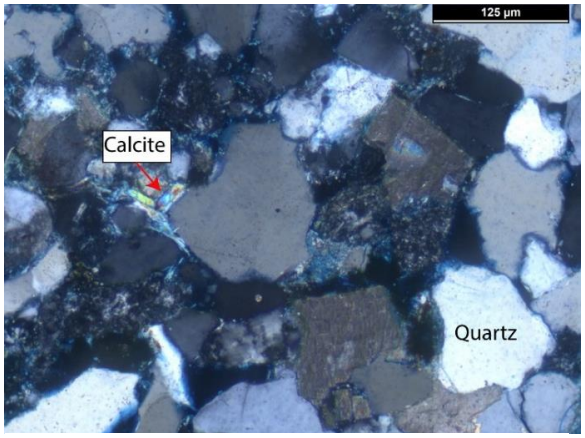

Figure 37: Calcite cement within rock sample MSw-B1 of the Salt Wash Member in cross polarized light.

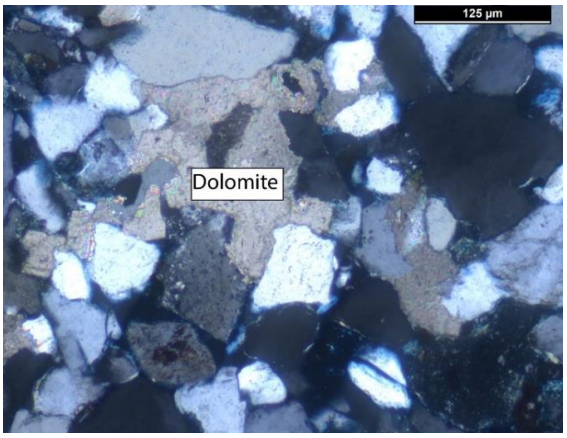

Figure 38: Irregular and porous dolomite cement within rock sample MSw-B1 in cross polarized light.

MSw-B1: Porosity

In sample MSw-B1, 19.4% of the sample is composed of pores. These include solution porosity, primary and secondary porosity, making up 42.3%, 51.5%, and 6.2% of porosity respectively (**Table 2**). Unlike the first sample, grains within sample MSw-B1 are very closely compacted with little to no pore space or cement between them. Secondary porosity within the sample is widely spaced enough and minimal where counting rarely landed on any large pores. However, there is a larger percentage of solution porosity found within dolomite cement (**Fig. 39**).

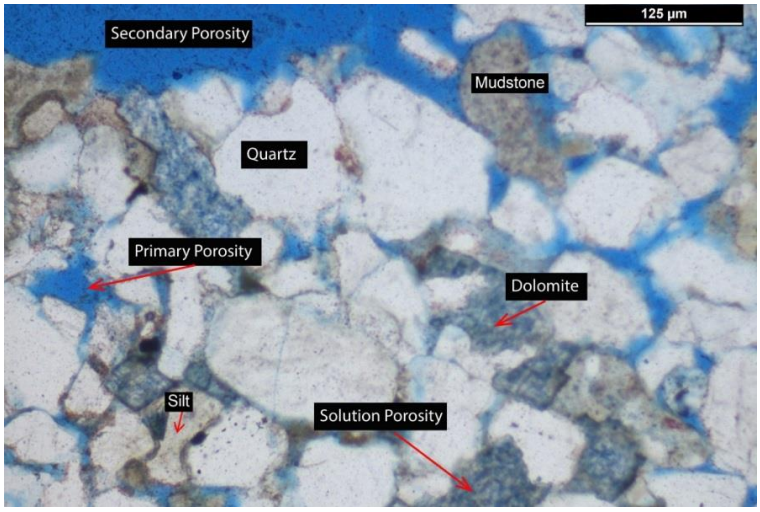

Figure 39: Porosity within sample MSw-B1 in plane polarized light. Blue dye was used to show pore space within the sample.

Table 2: Mineral composition distribution of sample MSw-B1, collected from the Salt Wash Member in area B, site B.2.

Mineral/Material	Points (400 Total)	Percent Total (%)	Type	Percent Type (%)
Quartz	222	55.5	67.6% Grains	82.1
Chalcedony	3	0.7		1
Mud	23	5.7		8.4
Silt	10	2.5		3.7
Microcline	13	3.2		4.7
Calcite	2	0.5	13% Cement	3.8
Dolomite	50	12.5		96.2
Solution Porosity	32	8.2	19.4% Porosity	42.3
Primary Porosity	40	10		51.5
Secondary Porosity	2	1.2		6.2

MSw-B2: Grains

Sample MSw-B2 is composed of 60% grains, 24.8% cement, and 15.2% porosity (**Table 3**). Of the grains, 89.2% are quartz, 6.6% are mudstones and siltstone, and 4.2% are microcline (**Table 3**) (**Fig. 41**). Like the previous sample, grains within sample MSw-B2 are very close together and there is little to no pore space. Quartz grains are fine to medium grained, sub-angular, and well sorted.

MSw-B2: Cement

Cements makes up 24.8% of the sample, including calcite, dolomite, and clay (**Table 3**). Calcite makes up 0.8% of cementation and is found filling porosity within large grains (**Table 3**). Dolomite makes up 89.5% of cementation and irregularly wraps around grains, filling large pore spaces (**Table 3**) (**Fig. 40, 41**). A clay cement makes up 9.7% of cementation (**Table 3**). In plane

polarized light, the cement appears dark brown to yellow and is found along the rims of quartz grains (**Figs. 41, 42**).

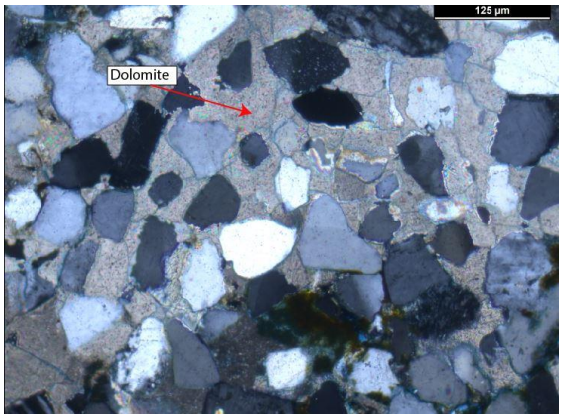

Figure 40: Dolomite grains within sample MSw-B2 in cross polarized light.

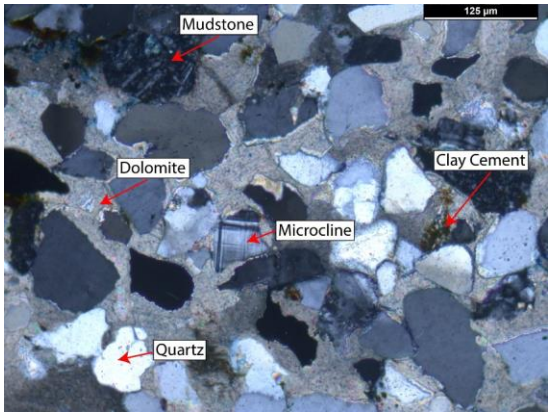

Figure 41: Grains and cement found within sample MSw-B2 in cross polarized light.

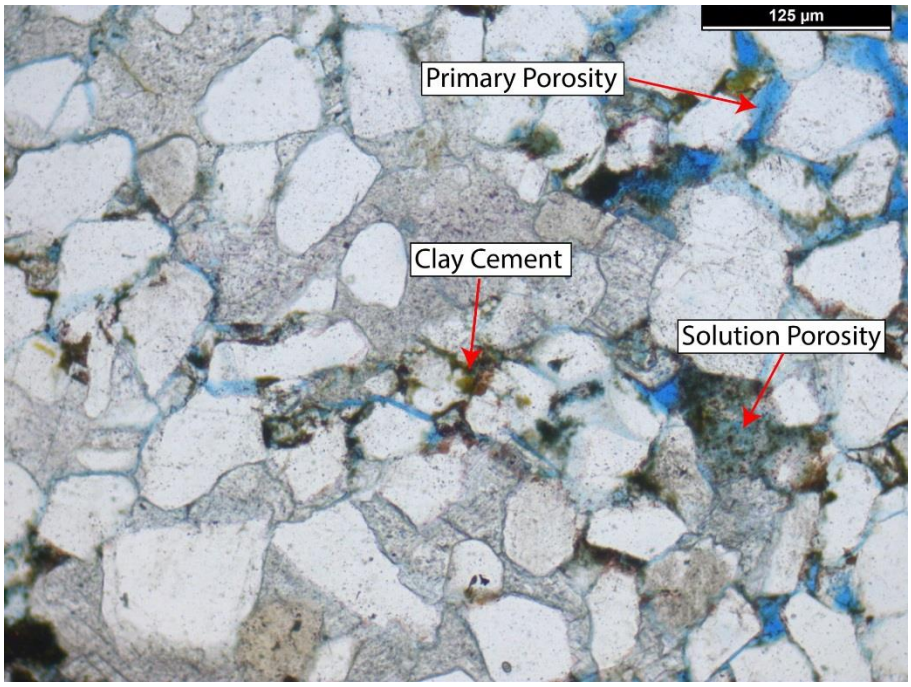

Figure 42: Clay cement and porosity types within sample MSw-B2 in plane polarized light.

MSw-B2: Porosity

Pores within sample MSw-B2 include solution porosity and primary porosity, making up 46.1% and 53.9% of porosity respectively (**Table 3**) (**Fig. 42**). Pores were identified with the use

of a blue dyed epoxy rosin. Solution porosity is identified as areas were grains appear to dissolve, allowing water to seep into the larger grain. Primary pores are those where the open space between grains was filled by water, but is no larger than the grains themselves. Lastly, any secondary pores that might have been present in the sample have been filled in by a poikilotopic dolomite cement (**Fig. 42**).

Table 3: Composition distribution of sample MSw-B2 collected from area B, site B.2, along the Salt Wash anticline axis.

Minerals/ Materials	**Points (400 Total)**	**Percent Total (%)**	**Type**	**Percent Type (%)**
Quartz	214	53.5	60% Grains	89.2
Mudstone	14	3.5		5.8
Siltstone	2	0.5		0.8
Microcline	10	2.5		4.2
Calcite	1	0.3	24.8% Cement	1.2
Dolomite	89	22.2		89.5
Clay Cement	9	2.3		9.3
Solution Porosity	28	7	15.2% Porosity	46.1
Primary Porosity	33	8.2		53.9

Comparison with Previous Studies

Previous studies carried out in the region determined that sandstones within the Salt Wash Member of the Morrison Formation were predominantly composed of quartz grains, with percentages ranging from 60-77% (Shawe, 1968; Breit and Goldhaber, 1996). This included mono- and polycrystalline quartz grains. Other less common minerals included chert, orthoclase, microcline, plagioclase, clay, calcite and (or) dolomite, barite, chlorite, hematite, biotite, muscovite, and pyrite. The petrographic analysis carried out by Shawe (1968) on the average

mineral composition of sandstones from Permian and Mesozoic formations in the Slick Rock district, Colorado, showed this same mineral distribution. However, it is important to note that several of the samples collected from the Salt Wash for analysis were close to uranium-vanadium deposits, resulting in higher-than-average amounts of calcite. From these studies, it was determined that carbonate minerals, silica, and clay often served as cementing agents (Shawe, 1968; Breit and Goldhaber, 1996). Sandstone lenses were also found to be more tightly cemented in the lower and middle units of the member as compared to the upper unit (Shawe et al., 1968). Thus, the upper units were subsequently found to be more porous. Additionally, calcite cement was observed more commonly in sandstones that were close to ore deposits or adjacent to mudstone layers (Shawe, 1968). The Salt Wash Member was also found to contain trace amounts of chalcedony cements and abundant quartz overgrowths. Quartz grains in contact with this cement lacked overgrowth, implying that chalcedony had formed early.

The samples collected in this study showed lower percentages of quartz grains as compared to those in other areas within the Salt Wash Members, with the highest percentage being 55.5% for sample MSw-B1 and the lowest being 38.5% for sample MSw-A (**Tables 1-3**). Additionally, chalcedony appeared as grains rather than cements (**Tables 1-3**) (**Fig. 32**). These grains were as large as quartz and sometimes coarser. Samples also showed a larger percentage of dolomite and calcite, not only as cement but as very fine individual grains within sample MSw-A. Following Shawe (1968) results, calcite and dolomite made up a combined average 8.2% sample percentage. In contrast, Sample MSw-B1 contained a combined percentage of 13% while MSw-B2 contained a combined percentage of 22.4%. The higher carbonate percentages are likely the result of diapir derived clasts that were eroded and picked up from the Paradox Formation and caprock during Morrison deposition.

Clay made up an average of 2.5% of the 38 samples collected by Shawe (1968), of which most were cements. This percentage is very minimal compared to the samples collected in this study, were units onlapped salt and Paradox Formation shales and gypsum. In sample MSw-A, clay and silt grains were found as large, sub-angular grains that made up 14.3% of the sample. These large grains contained multiple smaller grains within them, such as quartz, hematite, and gypsum. In samples MSw-B1 and MSw-B2, clay made up 8% and 4% of the sample respectively. As with the carbonates, the erosion of the underlying beds resulted in higher-than-normal percentages of clay and silt, both as cement and grains.

The samples analyzed in this study showed a higher-than-average porosity percentage, ranging from 15-19% of the sample. Fluids likely continued to flow through the area after Morrison deposition, resulting in a high percentage of solution porosity in soft grains and cements or completely eroding grains to form secondary pores. Sample MSw-A is a good example where many large grains dissolved or eroded completely, leading to a high percentage of secondary porosity. Carbonate cements, were not completely dissolved. However, solution porosity is dominant. This is more evident in samples MSw-B1 and MSw-B2 (**Figs. 39, 40, 41**).

Discussion

Area A: Paleo-canyon

Rock samples collected from the basal strata of the Morrison Formation contain diapir-derived detritus, such as green-clay chips and carbonate pebbles (**Fig. 13**). These are the result of erosion of the diapir margin and megaflap by the first channels that flowed across it during the deposition of the Morrison Formation. This indicates that the Morrison Formation was deposited directly on top of the salt diapir and not faulted against it during crestal collapse due to salt dissolution as it was previously speculated (Gutiérrez, 2004; Guerrero et al., 2015). The lower beds of the Morrison Formation onlap the tilted strata flanking the diapir, indicating continued minibasin subsidence and diapir rise as the Morrison Formation was being deposited.

In area A, stratigraphic sections measured along the outcrop and the 3-D model created using photogrammetry show that the Morrison Formation incises at least 4 meters into the underlying strata to create a paleo canyon (**Figs. 9-12**). Therefore, the contact between the Morrison Formation and the underlying units isn't a flat depositional surface. The megaflap must have formed a topographic high. This implies erosion or salt-tectonic uplift of the megaflap prior to deposition. Because everywhere else in the area, the Morrison Formation rests on the thin Summerville Formation, which shows little change in thickness, tectonic uplift of flanks of Big Gypsum Valley relative to this minibasin can be inferred, in contrast to regional erosion.

This observation of an incised canyon also has implications for hydrocarbons when applied to similar areas deep within the earth's surface. Salt diapirs have been known to act as seals but are very difficult to image properly using seismic data. Therefore, it is important to recognize similar structures along diapir margins in areas with good outcrop exposure. Area A provides the opportunity to measure the sand to shale ratio in the margin and the likeliness for hydrocarbon

traps and seals. In this case, the megaflap is a good conduit for hydrocarbons to reach the surface and the angular unconformity between the underlying units and the Morrison Formation, plus the presence of the salt wall, has the potential to serve as a structural trap. However, data collected in this area indicates that the channels that deposited the Morrison strata incised into the underlying stratigraphy, breaching any potential traps that might've been found below. Additionally, the shales within the Salt Wash Member are laterally inconsistent, indicating that there is no effective seal in the paleo-canyon.

Salt Margin Folds

Correlation of stratigraphic sections and 3D models in sites B, C, and D show that the sandstone beds within the Salt Wash thin and onlap the flanks of synclines (**Figs. 16, 18, 19, 21, 23, 25**) This observation indicates that thickening in synclines is a depositional phenomena rather than structural thickening through deformation of the diapir. Thickening in fold hinges is a common result of bed parallel slip and folding that might be expected in folds as tight as those at areas B and D. However, depositional changes rather than internal deformation are observed (**Figs. 18, 19**). Detailed mapping of the area showed that there are no faults along the outcrops that would have resulted from dissolution collapse, except for possibly at area E, again indicating slow syndepositional deformation while sediments were not yet cemented (**Fig. 17**). Pinch-out of the lowest beds indicates that deformation began before deposition of the first sediment. Onlap of an irregular surface is observed in all the areas (**Fig. 15-19, 22-25, 29**).

Two rock samples, collected from the base strata of the Salt Wash Member in area B, also showed diapir-derived carbonate pebbles and thin shale clasts (**Figs. 17, 19**). Like in area A, this shows the erosion of the underlying strata by the channels that deposited the Morrison Formation

in the late Jurassic. Thus, the Morrison was deposited directly on top of the diapir rather than faulted against it.

If we were to analyze the geometries observed in areas B and C for petroleum exploration, we would be able to note that there are multiple locations that are possible outcrop analogues of reservoir and traps. Adjacent to the salt diapir, near-vertical to vertical dipping strata of the Chinle and Wingate Formation serves as a conduit for hydrocarbons. The porous sands of these units could serve as reservoirs against the unconformity between these older strata and the Salt Wash Member of the Morrison Formation. If the seal was not good, hydrocarbons could flow into the porous sandstones of the Salt Wash and be trapped by the laterally continuous and relatively thick shale beds of the Morrison Formation. The schematic in **Figure 43** outlines all of the possible reservoir and traps within area B. Overall, these includes, the crests of anticlines on units deposited on the salt, horn traps, pinch-out traps, and stratigraphic traps. If these geometries were observed surrounding the salt diapir, there are multiple zones that could potentially hold hydrocarbons.

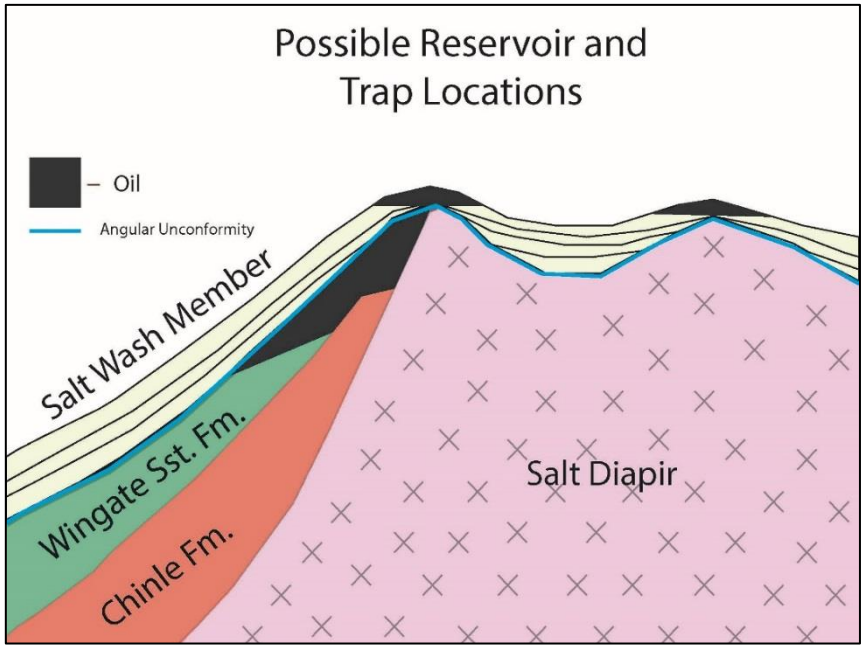

Figure 43: Schematic showing four possible analogues of reservoir and traps on the northeastern margin of the salt wall in Big Gypsum Valley, Colorado. Not drawn to scale.

Area D: Folds in the Brushy Basin

In area D, the Brushy Basin is folded into an anticline-syncline couple (**Figs. 24, 25**). Here, the Paradox Formation is covered by Quaternary alluvium adjacent to the Morrison outcrops. However, folding patterns similar to those of the Salt Wash can be observed on this upper unit of the Morrison Formation, where the scattered outcrops exhibit beds that pinch out against overlying beds and Quaternary alluvium. Additionally, dips in the Brushy Basin beds decrease away from the salt wall to the southwest from the folded zone into the Disappointment minibasin. Paleocurrent data collected on trough cross beds within the Brushy Basin showed that flow direction during deposition was to the southwest (**Fig. 14**). This indicates that during the deposition of the Brushy Basin, the Disappointment minibasin was lower in elevation than the salt wall. Thus, the salt diapir had risen above the minibasin sometime between the deposition of the Salt Wash and the Brushy Basin. A large normal fault can also be observed to the northwest of area D but does not extend onto the folded zone (**Fig. 14**). Thus, the observed folding patterns are likely the result of diapir rise adjacent to the outcrops during the deposition of the Brushy Basin.

Paleocurrent Measurements

Paleocurrent data collected along trough cross beds within unit 3 of the Salt Wash show that the meandering streams that deposited the Morrison Formation were flowing to the northeast across the diapir (**Fig. 14**). Therefore, the Disappointment minibasin to the southwest was topographic higher than the diapir during Morrison deposition. This direction of flow (northeast) matches the flow direction determined for the Slickrock District by Shawe et al. (1968) along festoon bedding sets and other cross-stratified structures, channel scours, current lineations, and current ripple marks within the Salt Wash Member (Shawe et al., 1968). This is consistent with the data collected from the Salt Wash on the southwestern margin of the diapir, indicating that the stratigraphy is correlatable to the Morrison strata in the adjacent areas flanking the diapir.

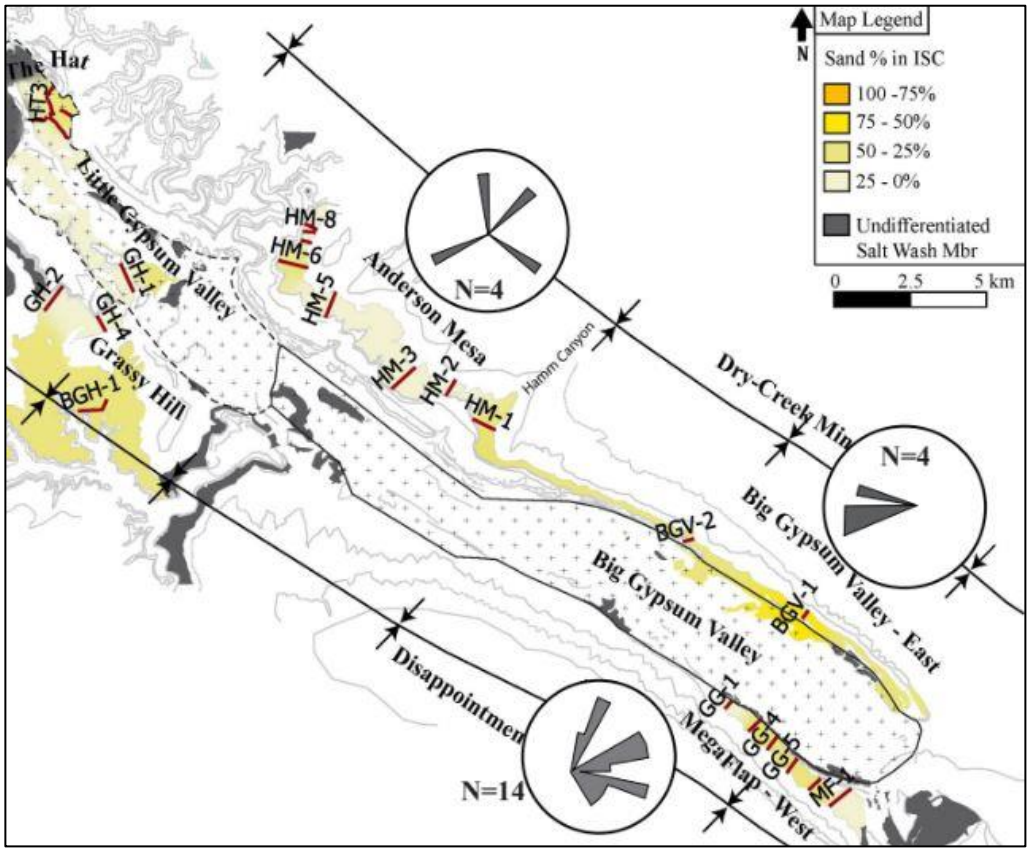

Figure 44: Geologic map of Gypsum Valley showing the paleocurrent measurements and sand percentages of unit 3 of the Salt Wash Member taken by Claire Bailey (2020).

Paleocurrent measurements taken by Claire Bailey on unit 3 of the Salt Wash, labeled as Isolated Sandstone Channels (ISC) in **Figure 44**, shows that sediment transport in Big Gypsum Valley is along the diapir margin (Bailey, 2020). Data were collected from the entire thickness of the Salt Wash and from 9 stratigraphic sections (**Fig. 44**). Bailey interpreted these results as being influenced by relative diapiric rise that directed channels subparallel to the salt wall margin rather than the regional flow direction to the northeast. She did not collect data from the study area for this thesis. Paleocurrent data collected on area A in this study showed a regional flow direction to the northeast. This indicates that flow went across the diapir, which was a topographic low during Morrison deposition. For area B, flow was to the southeast, along the diapir margin and parallel to the fold axis within the Morrison Formation. These results are generally opposite to the data collected by Claire Bailey (2020) and show much less dispersion. This is interpreted to result from the influence of the folding in area B, which had significant influence on channel direction. This is also compatible with the pinch-out of channels along syncline margins, indicating that channels were directed down the axes of folds.

Thin Sections

Petrographic samples contained a lower quartz percentage and higher clay, microcline, chalcedony, calcite, and dolomite percentage than the average values from Shawe's (1968) petrographic analysis on the Salt Wash Member in the Slick Rock district, Colorado. According to analysis by Shawe (1968) and Breit and Goldhaber (1996), sandstones within the Salt Wash were characterized for having dolomite and clay cements, making up 8.4% and 2.5% of the sample respectively. However, strata onlapping Paradox caprock and gypsum in this study showed large clay grains with interbedded gypsum crystals, making up between 4 to 14% of the samples. The higher-than-average clay and carbonate content is likely due to the erosion and mixing of Paradox shale and caprock during Morrison deposition. In the samples, grains were surrounded by four different types of cementation. These included quartz overgrowths, a thin clay cement, radial

quartz, and a coarse-grained quartz that filled out any remaining pores. The samples also showed a higher percentage in porosity, indicating that flowing fluid likely eroded a high amount of soft grains from the salt beds, such as clay and silt, resulting in solution porosity, primary, and secondary pores. Carbonate cements also contain a very high percentage of solution porosity, indicating fluid flow after cementation breaking down the rock further.

Conclusions

Results from this study indicate that diapiric salt movement continued through at least the late Jurassic during Salt Wash deposition. However, similar folding in the Brushy Basin is evident on the southwestern margin of the salt wall (**Fig. 24, 25**). The observed folding patters within the Brushy Basin would require that the diapir still be rising near the outcrops during deposition. The 3-D outcrop models and stratigraphic correlations carried out in areas B, C, and D illustrate that sandstone beds within the Salt Wash thin and onlap the flanks of synclines, with lateral changes of 3 to 4 meters. This observation indicates that thickening in synclines is a depositional phenomena rather than structural thickening due to deformation of the diapir through dissolution. Pinch out of the lowest beds of the Morrison Formation against Paradox caprock and gypsum shows that deformation began before deposition of the first sediment. Onlap of beds against the salt and older strata further indicate that deformation of both the salt and the overlying strata was syndepositional. The lack of faulting from the salt onlap to where the beds dip in to that adjoining minibasins confirms that much of the Morrison Formation is in place and has, at least locally, not been dropped into its present location through diapir dissolution fault collapse as previously thought.

Diapir derived clasts found within the basal units of the Salt Wash Member of the Morrison Formation also imply that the diapir was being eroded in areas adjacent to the areas of Salt Wash deposition. Petrographic analysis showed that samples sitting on salt contained a higher-than-average carbonate and clay content as grains and cement. These high percentages are likely due to the added material derived from Paradox shales and dolomites which were eroded and picked up during Morrison deposition. Samples also showed a higher percentage of porosity as compared to samples collected by Shawe (1968) in his study of the Salt Wash away from any salt wall. This indicates that fluid was present during sediment cementation and much of the soft clay and silt

within the sandstones were being dissolved or completely removed, resulting in high solution porosity, primary, and secondary pores within the collected samples.

References

Amador, C.M., Schurger, S.G., and Miller, B.L., 2009, Andy's Mesa Unit, San Miguel County, Colorado, *in* Houston, W.S., Wray, L.S., and Moreland, P.G. eds., The Paradox Basin Revisited - New Developments in Petroleum Systems and Basin Analysis, Rocky Mountain Association of Geologists, p. 497–518, http://archives.datapages.com/data/rocky-mtn-geologist-pubs/data/005/005001/497_rmag-bk0050497.htm (accessed March 2015).

Andrie, J.R., Giles, K.A., Lawton, T.F., and Rowan, M.G., 2012, Halokinetic-sequence stratigraphy, fluvial sedimentology and structural geometry of the Eocene Carroza Formation along La Popa salt weld, La Popa Basin, Mexico: Geological Society, London, Special Publications, v. 363, p. 59–79, doi:10.1144/SP363.4.

Baars, D.L., and Stevenson, G.M., 1981, Tectonic evolution of western Colorado and eastern Utah, *in* Western Slope (Western Colorado), New Mexico Geological Society Guidebooks, v. 32, p. 105–112.

Bailey, Claire, 2020. Halokinetic Influence on Fluvial Depositional Patterns in the Salt Wash Member of the Jurassic. University of Texas at El Paso. Ph.D. Dissertation in progress.

Bailey, Claire, 2020. Personal communication.

Morrison Formation, Gypsum Valley Salt Wall, Paradox Basin, Colorado

Banham, S.G., and Mountney, N.P., 2013, Evolution of fluvial systems in salt-walled mini-basins: A review and new insights: Sedimentary Geology, v. 296, p. 142–166, doi:10.1016/j.sedgeo.2013.08.010.

Barbeau, D.L., 2003, A flexural model for the Paradox Basin: implications for the tectonics of the Ancestral Rocky Mountains: Basin Research, v. 15, p. 97–115.

Breit, G.N., and Goldhaber, M.B., 1996, Diagenesis of Sandstones in the Morrison Formation within the Paradox Basin: Geology and Resources of the Paradox Basin, 1996, p. 14.

Cater, F.W., 1955a, Geology of the Gypsum Gap quadrangle, Colorado: Map GQ-59.: Geol. Quad. U.S. Geol. Survey GQ-59.

Cater, F.W., 1955b, Geology of the Joe Davis Hill quadrangle, Colorado: Geol. Quad. U.S. Geol. Survey GQ-66.

Cater, F.W., and Craig, L.C., 1970, Geology of the Salt Anticline region in southwestern Colorado, with a section on stratigraphy.: Geol. Quad. U.S. Geol. Survey PP-637, 84 p.

Condon, S.M., 1992, Geologic framework of pre-Cretaceous rocks in the Southern Ute Indian Reservation and adjacent areas, southwestern Colorado and northwestern New Mexico: US Geological Survey Bulletin, v. 1505-A, p. 53.

Condon, S.M., 2000, Geology of the Pennsylvanian and Permian Cutler Group and Permian Kaibab Limestone in the Paradox Basin, Southeastern Utah and Southwestern Colorado: U.S. Geological Survey, Bulletin, v. 2000-P, 59 p., http://ulpeis.anl.gov/documents/dpeis/references/pdfs/Condon_1997.pdf (accessed March 2015).

Deatrick, K.T., 2019, Sequence Stratigraphy, Diagenesis, and Depositional Facies of an Exposed Megaflap: Pennsylvanian Hermosa Group, Gypsum Valley Salt Wall, Paradox Basin, Colorado [M.S.]: The University of Texas at El Paso, 198 p., https://search.proquest.com/docview/2364243646/abstract/60336CBEA35A466DPQ/1 (accessed March 2020).

Deatrick, K., Giles, K., Langford, R., Rowan, M., and Hearon, T. Depositional Facies and Geometry of an Exposed Megaflap: Pennsylvanian Honaker Trail Formation, Gypsum Valley Salt Wall, Paradox Basin, Colorado, http://www.searchanddiscovery.com/abstracts/html/2015/90219gcags/abstracts/76.html (accessed September 2017).

DeCelles, P.G., and Currie, B.S., 1996, Long-term sediment accumulation in the Middle Jurassic − early Eocene Cordilleran retroarc foreland-basin system, *in* v. 24, p. 591–594.

Doelling, H.H., and Ross, M.L., 1998, Geologic map of the Big Bend 7.5' quadrangle, Grand County Utah.: Utah Geological Survey Geologic Map B-171, 29 p.

Elston, D.P., Shoemaker, E.M., and Landis, E., 1962, Uncompahgre front and salt anticline region of Paradox Basin, Colorado and Utah: AAPG Bulletin, v. 46, p. 1857–1878.

Escosa, F.O., Rowan, M.G., Giles, K.A., Deatrick, K.T., Mast, A.M., Langford, R.P., Hearon, T.E., and Roca, E., 2019, Lateral terminations of salt walls and megaflaps: An example from Gypsum Valley Diapir, Paradox Basin, Colorado, USA: Basin Research, v. 31, p. 191–212, doi:10.1111/bre.12316.

Ge, H., 1996, Kinematics and dynamics of salt tectonics in the Paradox Basin, Utah and Colorado: Field observations and scaled modeling [Ph.D.]: The University of Texas at Austin, 317 p., https://0-search.proquest.com.lib.utep.edu/pqdtglobal/docview/304274991/abstract/F7AEB38BE1C4109PQ/1.

Ge, H., and Jackson, M.P., 1998, Physical modeling of structures formed by salt withdrawal: Implications for deformation caused by salt dissolution: AAPG bulletin, v. 82, p. 228–250.

Ge, H., Jackson, M.P., and Vendeville, B.C., 1996, Extensional origin of breached Paradox diapirs, Utah and Colorado: field observations and scaled physical models: Utah Geological Association, p. 285–294.

Giles, K.A., and Lawton, T.F., 2002, Halokinetic sequence stratigraphy adjacent to the El Papalote diapir, northeastern Mexico: AAPG bulletin, v. 86, p. 823–840.

Giles, K.A., and Rowan, M.G., 2012, Concepts in halokinetic-sequence deformation and stratigraphy: Geological Society, London, Special Publications, v. 363, p. 7–31.

Grisi, K.C., 2018, Attributes of the Fisher Valley Megaflap and Comparison to the Gypsum Valley Megaflap, Paradox Basin, Utah and Colorado: Implications for Controls on Megaflap Formation [MS Thesis]: University of Texas at El Paso, 137 p.

Guerrero, J., Bruhn, R.L., McCalpin, J.P., Gutierrez, F., Willis, G., and Mozafari, M., 2015, Salt-dissolution faults versus tectonic faults from the case study of salt collapse in Spanish Valley, SE Utah (USA): Lithosphere, v. 7, p. 46–58, doi:10.1130/L385.1.

Gutiérrez, F., 2004, Origin of the salt valleys in the Canyonlands section of the Colorado Plateau: Geomorphology, v. 57, p. 423–435, doi:10.1016/S0169-555X(03)00186-7.

Hanshaw, B.B., and Hill, G.A., 1969, Geochemistry and hydrodynamics of the Paradox Basin region, Utah, Colorado and New Mexico: v. 4, p. 263-294.: Chemical Geology, v. 4, p. 263–294.

Hartley, A.J., Owen, A., Swan, A., Weissmann, G.S., Holzweber, B.I., Howell, J., Nichols, G., and Scuderi, L., 2015, Recognition and importance of amalgamated sandy meander belts in the continental rock record: Geology, v. 43, p. 679–682, doi:10.1130/G36743.1.

Hasiotis, S.T., 2004, Reconnaissance of Upper Jurassic Morrison Formation ichnofossils, Rocky Mountain Region, USA: paleoenvironmental, stratigraphic, and paleoclimatic significance of terrestrial and freshwater ichnocoenoses: Sedimentary Geology, v. 167, p. 177–268, doi:10.1016/j.sedgeo.2004.01.006.

Hazel, J.E., 1994, Sedimentary response to intrabasinal salt tectonism in the Upper Triassic Chinle Formation: US Geological Survey Bulletin 2000-F, 30 p.

Heness, E.A., 2016, Salt tectonic controls on facies and sequence stratigraphy of the Triassic Chinle Formation, Gypsum Valley Salt Wall, Colorado [M.S.Thesis]: The University of Texas at El Paso, 156 p., https://0-search-proquest-com.lib.utep.edu/pqdtglobal/docview/1805065474/abstract/483F51F7672348D4PQ/1 (accessed February 2018).

Hudec, M.R., 1995, The Onion Creek salt diapir: an exposed diapir fall structure in the Paradox basin, Utah. 125-134., *in* Travis, C.J., Harrison, H., Vendeville, B.C., Hudec, M.R., and Perkins, B.F. eds., Salt, sediment, and hydrocarbons, 16th Annual Research Conference Program and Extended Abstracts: Society of Economic Paleontologists and Mineralogists, Gulf Coast Section, p. 125–134.

Hudec, M.R., and Jackson, M.P.A., 2007, Terra infirma: Understanding salt tectonics: Earth-Science Reviews, v. 82, p. 1–28, doi:10.1016/j.earscirev.2007.01.001.

Huntoon, J.E., Dubiel, R.F., Stanesco, J.D., Mickelson, D.L., and Condon, S.M., 2002, Permian-Triassic depositional systems, paleogeography, paleoclimate, and hydrocarbon resources in Canyonlands and Monument Valley, Utah, *in* GSA Field Guide 3: Science at the

Highest Level, Geological Society of America, v. 3, p. 33–58, http://fieldguides.gsapubs.org/cgi/doi/10.1130/0-8137-0003-5.33 (accessed March 2015).

Jackson, M.P.A., Schultz-Ela, D.D., Hudec, M.R., Watson, I.A., and Porter, M.L., 1998, Structure and evolution of Upheaval Dome: A pinched-off salt diapir: Geological Society of America Bulletin, v. 110, p. 1547–1573.

Kelley, V.C., 1958, Tectonics of the region of the Paradox Basin: Utah Geological Association, p. 31–38.

Kluth, C.F., 1986, Plate tectonics of the Ancestral Rocky Mountains: Part III. Middle Rocky Mountains, *in* Peterson, J.A. ed., Paleotectonics and sedimentation in the Rocky Mountain region, United States, American Association of Petroleum Geologists Memoir 41, p. 353–369.

Kluth, C.F., and Coney, P.J., 1981, Plate tectonics of the ancestral Rocky Mountains: Geology, v. 9, p. 10–15.

Kowallis, B.J., Christiansen, E.H., and Deino, A.L., 1991, Age of the Brushy Basin Member of the Morrison Formation, Colorado Plateau, western USA: Cretaceous Research, v. 12, p. 483–493, doi:10.1016/0195-6671(91)90003-U.

Mack, G.H., and Rasmussen, K.A., 1984, Alluvial-fan sedimentation of the Cutler Formation (Permo-Pennsylvanian) near Gateway, Colorado: Geological Society of America Bulletin, v. 95, p. 109–116.

Mast, A.M., 2016, The origin of anomalous carbonate units outcropping at the salt sediment interface of the southern end of Gypsum Valley Salt Wall, Paradox Basin, southwest Colorado [M.S.]: The University of Texas at El Paso, 199 p., https://0-search-proquest-com.lib.utep.edu/pqdtglobal/docview/1876050813/abstract/D24FAE6CD6434471PQ/1 (accessed February 2018).

Matthews, W.J., Hampson, G.J., Trudgill, B.D., and Underhill, J.R., 2007, Controls on fluviolacustrine reservoir distribution and architecture in passive salt-diapir provinces: Insights from outcrop analogs: AAPG bulletin, v. 91, p. 1367–1403.

McFarland, J.C., 2016, Structural and stratigraphic development of a salt-diapir shoulder, Gypsum Valley, Colorado [M.S.Thesis]: The University of Texas at El Paso, 106 p., https://0-search-proquest-com.lib.utep.edu/pqdtglobal/docview/1803590334/abstract/8A8B53FAAF554422PQ/1 (accessed February 2018).

Nuccio, V.F., and Condon, S.M., 1996, Burial and Thermal History of the Paradox Basin, Utah and Colorado, and Petroleum Potential of the Middle Pennsylvanian Paradox Formation: US.S. Geological Survey Bulletin 2000-O, 41 p., http://archives.datapages.com/data/uga/data/067/067001/57_ugs670057.htm (accessed March 2015).

Owen, A., Nichols, G.J., Hartley, A.J., Weissmann, G.S., and Scuderi, L.A., 2015, Quantification of a Distributive Fluvial System: The Salt Wash DFS of the Morrison Formation, SW U.S.A.: Journal of Sedimentary Research, v. 85, p. 544–561, doi:10.2110/jsr.2015.35.

Rasmussen, Donald.L., 2016, Discovery of an Exposed Early Triassic Namakier (salt Glacier) on the West Flank of the Onion Creek Diapir in Grand County, Utah, doi:10.1130/abs/2016AM-286899.

Ronson, R.B., 2018, Facies Changes Associated with Formation of an Extensive Salt Shoulder by the Coastal and Eolian Carmel and Entrada Formations, Gypsum Valley, Colorado [M.S.]: The University of Texas at El Paso, 142 p., http://0.search.proquest.com/dissertations/docview/2111273760/abstract/14E13374BAC64419PQ/1 (accessed September 2019).

Rowan, M.G., Giles, K.A., Hearon IV, T.E., and Fiduk, J.C., 2016, Megaflaps adjacent to salt diapirs: AAPG Bulletin, v. 100, p. 1723–1747, doi:10.1306/05241616009.

Rowan, M.G., Lawton, T.F., Giles, K.A., and Ratliff, R.A., 2003, Near-salt deformation in La Popa basin, Mexico, and the northern Gulf of Mexico: A general model for passive diapirism: AAPG Bulletin, v. 87, p. 733–756.

Rowan, M.G., and Vendeville, B.C., 2006, Foldbelts with early salt withdrawal and diapirism: Physical model and examples from the northern Gulf of Mexico and the Flinders Ranges, Australia: Marine and Petroleum Geology, v. 23, p. 871–891, doi:10.1016/j.marpetgeo.2006.08.003.

Shawe, D.R., 1968, Petrography of sedimentary rocks in the Slick Rock district, San Miguel and Dolores Counties, Colorado: U.S. Geol. Survey Prof. Paper 576-B, 34 p.

Shawe, D.R., 1970, Structure of the Slick Rock district and vicinity, San Miguel and Dolores Counties, Colorado, *in* US. Geol. Survey Prof. Paper 576-C, p. 18.

Shawe, D.R., Simmons, G.C., and Archibold, N. l., 1968, Stratigraphy of Slick Rock District and vicinity, San Miguel and Dolores Counties, Colorado.: US. Geological Survey U.S. Geological Survey Professional Paper 576-A, A1–A108 p.

Stokes, W.L., 1944, Morrison formation and related deposits in and adjacent to the Colorado Plateau: Geological Society of America Bulletin, v. 55, p. 951–992, doi:10.1130/GSAB-55-951.

Stokes, W.L., and Phoenix, D.A., 1948, Geology of the Egnar - Gypsum Valley Area, San Miguel and Montrose Counties Colorado: U.S. Geological Survey OM-93 Oil and Gas Investigations Map.

Trudgill, B.D., 2011, Evolution of salt structures in the northern Paradox Basin: controls on evaporite deposition, salt wall growth and supra-salt stratigraphic architecture: Evolution of salt structures in the northern Paradox Basin: Basin Research, v. 23, p. 208–238, doi:10.1111/j.1365-2117.2010.00478.x.

Trudgill, B.D., Banbury, N., Underhill, J., and Post, P.J., 2004, Salt evolution as a control on structural and stratigraphic systems: Northern Paradox foreland basin, southeast Utah, USA, *in* Salt-Sediment Interactions and Hydrocarbon Prospectivity: Proceedings, Gulf Coast Section SEPM Foundation (Society for Sedimentary Geology), Annual Bob F. Perkins Research Conference, SEPM, v. 24, p. 669–700, http://gcsproceedings.sepmonline.org/content/gcs024/1/SEC46.body.pdf (accessed September 2017).

Tyler, N., and Ethridge, F.G., 1983, Depositional setting of the Salt Wash Member of the Morrison Formation, Southwest Colorado: Journal of Sedimentary Research, v. 53, p. 67–82, doi:10.1306/212F8157-2B24-11D7-8648000102C1865D.

Venus, J.H., Mountney, N.P., and McCaffrey, W.D., 2015, Syn-sedimentary salt diapirism as a control on fluvial-system evolution: an example from the proximal Permian Cutler Group, SE Utah, USA: Basin Research, v. 27, p. 152–182, doi:10.1111/bre.12066.

Whidden, K.J., Lillis, P.G., Anna, L.O., Pearson, K.M., and Dubiel, R.F., 2014, Geology and total petroleum systems of the Paradox Basin, Utah, Colorado, New Mexico, and Arizona: Mountain Geologist, v. 51, p. 21.

White, M.A., and Jacobson, M.I., 1983, Structures associated with the southwest margin of the ancestral Uncompahgre Uplift (W. R. Averett, Ed.): , p. 33–39.

Vita

On 2011, Alondra Soltero enrolled into Mission Early College High School upon being recommended by her instructors due to her academic excellence. As part of the early college program, she began attending college courses at the Mission Del Paso Community College. She graduated with her Associates of Arts Degree on May 29, 2014, and began taking courses at the University of Texas at El Paso (UTEP) the upcoming semester. Alondra graduated with her High School Diploma on 2015 on the top 10 of the graduating class and began as a full-time student at UTEP. On her last semester as an undergraduate, Alondra worked as a Research Assistant at the university on the USDA Water Sustainability Project. She graduated with her Bachelor of Science Degree in Geology on May 13, 2017, where she earned the "Outstanding Graduating Senior in Geology" award and the Summa Cum Laude achievement. On Fall 2017, Alondra enrolled in the graduate program at UTEP to pursue a Master of Science Degree in Geology. On December 2018, she went on to graduate with the Geographic Information Science and Technology (GIST) Certificate. During her graduate education, Alondra worked as a Teaching Assistant and became an active member of the Institute of Tectonic Studies group within the university. She went on to present her thesis research at multiple conventions, such as the Rocky Mountain Rendezvous conference, AAPG Annual Convention and Exhibition, and Salt Sediment Interaction Research Consortium. While a graduate student, she received research grants from the American Association of Petroleum Geologists (AAPG), Geological Society of America (GSA) and Western Texas Geological Society (WTGS).

Contact Information: soltero.alondra@yahoo.com